Universidade de Aveiro Departamento de Engenharia Mecânica
2012

DANIELA SOFIA MARTINS DOS SANTOS

PARAMETRIC COMPUTATIONAL SIMULATIONS OF UNIPORE CELLULAR STRUCTURE SUBJECTED TO COMPRESSIVE LOADING

Dissertação apresentada à Universidade de Maribor para cumprimento dos requisitos necessários à obtenção do grau de Mestre em Engenharia Mecânica, realizada sob a orientação científica do Professor Doutor Zoran Ren,e do Professor assistente Matej Vesenjak, Professores do Departamento de Engenharia Mecânica da Universidade de Maribor.

Aos meus pais e a minha irmã Sónia.

o júri

presidente

Prof. Doutor Miran Ulbin
Professor Auxiliar da Universidade de Maribor

Prof. Doutor Zoran Ren
Professor da Universidade de Maribor

Prof. Doutor Matej Vesenjak
Professora Auxiliar da Universidade de Maribor

Agradecimentos

Àо Professor Doutor Zoran Ren e ao Professor doutor Matej Vesenjak, orientadores desta tese pela a disponibilidade e osensinamentos constantes, que contribuíram para a concretização deste trabalho.

À Doutora Isabel Duarte pela a confiança, o encorajamento, ensinamentos e sugestões, que contribuíram de forma determinante para a concretização deste trabalho, conferindo um valor à investigação que, de outra forma, não teria sido possível.

À Universidade de Maribor e à Faculdade de Engenharia técnica, o apoio nesta investigação.

Ao Professor Doutor Gil Andrade-Campos pelo incansável apoio e pela disponibilidade que tanto facilitaram o percurso final desta investigação.

À Professora Doutora Mónica Oliveira, pelo carinho,atenção e disponibilidade que contribuiram decisivamente para a finalização desta tese.

Ao Professor Doutor Matej Borovinšek pelos ensinamentos iniciais e pelo apoio e disponibilidade constantes no decorrer desta investigação.

Ao Aljaž Kovačičpela atenção e cuidado, pelas explicações e sugestões, que tanto facilitaram a integração com a língua e procedimentos eslovenos.

Ao Ricardo Carranca, pelas sugestões sensatas, pela amizade incondicional e, finalmente, pelas ajudas que contribuiram definitivamente para a boa conclusão deste trabalho.

Ao André Silva, pelo apoio e constante motivação, por todos os momentos de encorajamento, ao Nino pelas revisões em esloveno, ao Tedi pelo companheirismo no trabalho de investigação, à Mateja e ao Zvonimir porque sem eles teria sido mais difícil.

Aos amigos que mesmo distantes estiveram sempre presentes ao longo de todo este processo. À Rita, a sua incansável amizade sem horários e em qualquer circunstância. Ao Nuno, ao Luís e à Catarina e ao Carlos, por estar sempre presente.

Aos meus pais, o apoio incondicional e coragem que sempre me transmitiram. À minha irmã, pelo apoio incondicionalmente entusiasta, por dividir todas as dificuldades e simplificar todos os obstáculos. E por inumeráveis outras circunstâncias, enfim, por ser minha irmã

A todos, os meus sinceros agradecimentos.

Univerza v Mariboru
Fakulteta za strojništvo

universidade de aveiro

PARAMETRIC COMPUTATIONAL SIMULATIONS OF UNIPORE CELLULAR STRUCTURE SUBJECTED TO COMPRESSIVE LOADING

Master Thesis

Student Name: Daniela Sofia Martins dos Santos

Study Programme: Master Study Programme of Mechanical Engineering

Supervisor: red. prof. dr. Zoran REN

Co-supervisor: doc. dr. Matej VESENJAK

Maribor, December 2012

Univerza v Mariboru

Fakulteta za strojništvo

Num: S-BM0016
Date: Maribor, April 10th, 2012

DECISION ON MASTER THESIS TOPIC

Ms. Daniela Sofia Martins Dos Santos, Erasmus student from the University of Aveiro, Portugal, satisfies the set conditions of the Master (2nd level) study programme of Mechanical Engineering and is allowed to prepare her master thesis.

The topic of the master thesis falls under the heading of Computational Solid Mechanics course, Engineering computer modelling study field.

Mentor: Prof. Dr. Zoran Ren
Co-mentor: Asist. Prof. Dr. Matej Vesenjak

Expiry date of master thesis topic: April 10th, 2013

Master thesis title: **Parametric computational simulations of UniPore cellular structure subjected to compressive loading**

Master thesis content:

- study of literature on mechanical behaviour of cellular materials;
- preparation of computational models of regular and irregular UniPore material for parametric computational simulations;
- parametric non-linear computational simulations of UniPore material behaviour under rising outer and inner constant pressure and outer force loading in different directions with FE programme system Abaqus;
- analysis of computational results and derivation of conclusions.

The master thesis is to be prepared in accordance with "Guidelines for preparation of the Master Thesis" and submitted in three copies no later than September 30th, 2012.

Head of Chair for Constructions and Design:
Prof. Dr. Jože Flašker

Dean:
Prof. Dr. Niko Samec

Mentor:
Prof. Dr. Zoran Ren

UNIVERZA V MARIBORU FAKULTETA ZA STROJNIŠTVO 7

DECLARATION

Undersigned Daniela Sofia Martins dos Santos declare that this Master Thesis:

- is the result of my own investigations, except where specific references to other investigations are made, and was individually prepared under supervision of prof. dr. Zoran REN and co-supervision of doc. dr. Matej VESENJAK;
- has not previously been accepted in substance for any degree and is not being concurrently submitted in candidature for any degree at any other university;
- can be made publicly available in the Library of Technical Faculties of University of Maribor.

Maribor, December 18th, 2012 Signature: Daniela Santos

ACKNOWLEDGMENTS

I wish to express my gratitude to my mentor, Dr. Zoran Ren and co-mentor Dr. Matej Vesenjak. I express, as well, deep appreciation for all the attention given by investigators in mechanical engineer faculty from Maribor University. Likewise, the advisement and support mostly from Dr. Isabel Duarte, and also Dr. Mónica Oliveira and Dr. Gil Campos from Mechanical engineering department of Aveiro University is particularly acknowledged.

PARAMETRIC COMPUTATIONAL SIMULATIONS OF UNIPORE CELLULAR STRUCTURE SUBJECTED TO COMPRESSIVE LOADING

Key Words: Porous Materials, UniPore structure, Finite Element Analysis, Mechanical Properties

UDK: 531/533:519.61/.64(043.2)

ABSTRACT

The thesis study focuses on behaviour of a newly developed cellular UniPore structure with unidirectional pores under transversal and longitudinal loading. The computational model of the cellular structure was based on reconstructed irregular geometry of the manufactured specimens and analysed using ABAQUS. The mechanical properties have been studied using parametric computational simulations considering several material and geometrical parameters. Numerical tests provide data of compressive behaviour of UniPore structures and mechanical properties, such as elastic modulus or yield strength.

CONTENTS

LIST OF FIGURES

1. INTRODUCTION

With this study it is intended to present a new material – UniPore, where its main ambition lies upon the classification of the material according to the usual topics used to define a given foam material.

UniPore material has been recently developed at Shock Wave and Condensed Matter Research Centre at Kumamoto University in Japan. UniPore belongs to a class of new and until present an uncharacterized cellular material.

Properties of cellular solids have been extensively investigated for each specific type of cellular solid, however there is still much to explore, catalogue and accomplish. The characteristics of foams are defined by its relative density and base material properties. Structure, distribution, size and shape of cells are also properties that make part of the foam characterization, as Ashby states it in his book about Metal Foams. [1]

1.2 Description of the problem

The prototype samples in this study are manufactured by compressive blast loading of the outer copper pipe containing tightly packed thin-walled copper pipes of much smaller diameter, filled with paraffin. Compressive blast loading causes compaction of the pipes, which are blast welded along contact surfaces during the production process.

Cellular solids have physical, mechanical and thermal properties which can be assessed by the same methods as those used for fully dense solids. As it will be specified later, mechanical properties depend primarily upon the relative density of the foam and on the material of which it is made, computational models will consider also other material types, besides copper (i.e. aluminium, steel) and also elastoplastic behaviour will be considered in the analysis.

As the process used to create this material does not enable a strict control of the pore geometry, and this will influence the characteristics of the cellular material, the investigation on variation of the pore size is pertinent in this matter. As the pore geometry, also the porosity influences the cellular structure response, therefore it is also relevant to investigate the material behaviour with different porosities.

1.2 Objectives

UniPore material has a structure with some particular properties, which are very attractive for building efficient modern lightweight structures. Due to its novelty is, however, fundamental to assess the characterization of mechanical characteristics of UniPore material, both by experimental and computational means. This thesis topic is dedicated to the latter. Full understanding of the material behaviour is fundamental to integrate each cellular solid in the appropriate application. This mechanical problem can be studied through models that predict

their compressive deformation behaviour. Saving unnecessary experimental procedures in what concerns to the manufacturing processes is the reason to resort to numerical simulations.

The specimen properties depend most directly on those of the material that they are made off, and on their relative density. Moreover, it is also indicated that properties are influenced by structure. [1] The numerical simulations performed in this thesis intended to contribute with some clarification for this matter, gathering information without undergoing experimental essays. Accordingly, it will be studied how the porosity relates with the material behaviour under compression, both in parallel and perpendicular direction of the pores. To obtain the material deformation behaviour under the imposed load will be performed a set of static tests, depending on previously defined material deformation. These numerical tests will provide relations between the architecture of the sample and mechanical properties, such as elastic modulus or yield strength. The variation of the sample base material will, as well, offer knowledge on how this fact relates with the stiffness of the specimen.

All the referred items points towards the fact that the mechanical properties of cellular materials with a given density can be optimized by changing the internal architecture. The intent of the present investigation is to start a path in order to define the proper application of UniPore material, understanding its behaviour under compression. Moreover, it is intended to comprehend which is the relative influence of the structural geometry design of the pores on the achieved mechanical properties. Therefore, a proper characterization in order to assess both Young's modulus and compressive yield stress is determinant.

2. CELLULAR MATERIALS

Cellular arrangement of matter is a building principle of the nature. Human trabecular bone, wood, cork, the hexagonal bees' honeycombs, Figure 2.1, plant stems or glass sponges are some of the examples of the natural cellular materials. The structural use of natural cellular materials by man is as old as history itself. Transporting the captivating structures and unique mechanics of natural cellular materials, man has been made many artificial cellular structures from metals, ceramic and polymers. [1, 2]

Figure 2.1 - Hexagonal honeycomb existing in nature.

The combination of material and structural properties results in a set of completely new properties of solids. Potentially new applications have been identified in the fields of energy saving, lightweight construction, novel and efficient conversion concepts or biomedical repair functions. Nowadays, physicists, chemists, material scientists and engineers explore those combinations by mixing cellular structures of all material classes. Among man-made cellular materials, metal foams are a class of materials with low densities and attractive thermal, mechanical, electrical and acoustic properties. The history of metal foams dates back to the 1940s. The very first metal foam was processed by Benjamin Sosnick in 1948. Many patents were issued from the late 1950s to the 1970s and many variants of foaming processes were proposed. As hardly any publication was ever issued beside these patents, it is difficult to assess whether all the ideas suggested actually worked. A second upsurge of scientific activities started in the late 1980s headed to the re-establishment of some of the old techniques and to a far extensive publication activity. [3, 4, 5, 6]

The designation of metallic foam is, nowadays, adopted for several sorts of metallic materials that contain voids. In opposition to an idealized unit cell, most cellular materials have imperfections and in their microstructure, there is lack of homogeneity, such as different cell wall thickness, missing cell walls, filled cells and irregular organization of cell walls. [1]

Foams are not usually characterized by regular packing of equivalent units; instead, they contain cells of different sizes and shapes with variable number of faces and edges,

creating a stochastic geometry. In most cases, cellular materials are anisotropic, due to the lack of homogeneity of the cell wall. In fact, most of the foams manufactured by man are anisotropic. The material is said to be an open-cell cellular structure if the cells that composes the foam is connect through open faces. If the faces are solid as well, so that the pores are sealed off from their neighbours, it is said to be a closed-cell cellular structure. [7, 8]

Inside the metallic structures group there is a special classification for metallic structures having gaseous voids dispersed throughout the material, it is designated as low density cellular material. The referred voids contribute to a density reduction and, in the same time, improving strength, impact-absorption, and acoustic insulation.

Low-density cellular materials are metallic bodies in which any kind of gaseous voids are dispersed. The main advantage attainable from cellular materials is the high strength complemented with a relatively low mass. Cellular materials can also offer large stiffness, improved impact-absorption, thermal and acoustic insulation to their applications. [9]

The ability to select the material type and the possibility to predict an approximate geometry for the cellular material make the ideal for the ultimate manufacturing process, furthermore, this would consent prediction of properties. [2, 8]

Designing the mesoscopic topology (the geometric arrangement of the solid phases and voids within a material or product on the size range of 0.1 to 10 mm) of cellular materials in order to successfully support and improve design objectives has been a research aim for several investigators. [10]

2.1 Classification of Cellular Materials

Several different types of cellular materials have resulted from the multiple decades of research dedicated to creating manufacturing processes capable of producing human-made cellular materials. Cellular materials are classified by the nature of placement of the internal voids – either stochastic (disordered) or deterministic (ordered), two examples of which are shown in Figure 2.2.

Both stochastic and deterministic arrangements have assemblies of cells with solid boundaries that can have beam like or plate like components. [7]

Disordered cellular materials have cells of random distribution, profile and morphology. Banhart distinguishes three types of stochastic cellular metals: porous metals, solid metal foams, and metal sponges. [9]

Porous metals are a special class of cellular metals in which the pores are characteristically round and are isolated from each other. While solid metal foams have closed, round, or polyhedral cells that are separated by thin films, metal sponges alternatively, have interconnected cavities throughout the structure. Hollow sphere foams are composed of miniature hollow spheres. Despite the disordered arrangement, they present a uniform cell size distribution improvement as well as regular cell shape. [11, 10]

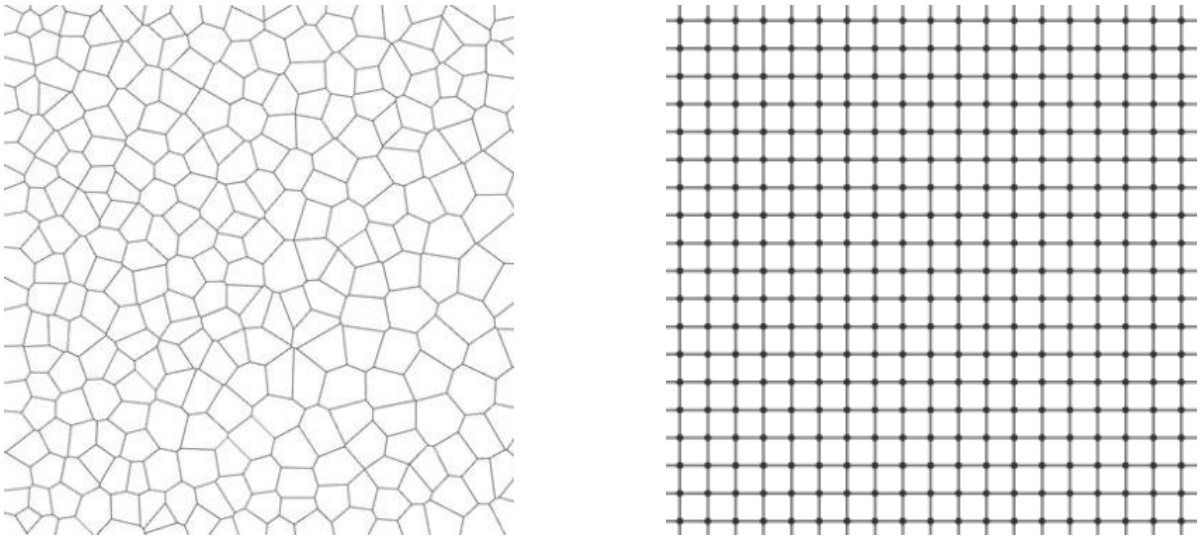

Figure 2.2 - Voronoi structure (stochastic arrangement) and square lattice (deterministic arrangement). [12, 13]

Up to the present time, honeycomb material and lattice group blocks, two different types of ordered metallic cellular structures have been successfully manufactured. These geometries demonstrated to have better stiffness and strength than the equivalents stochastic arrangements [7, 10]

Cellular solids are mentioned as having porosity under 0.7. Natural foams appear in the nature produced by plants (such as cork or balsa) and by animals (bone). Foams created by man are manufactured with ceramics, metals or polymers. [1]

Open cell structure presents interconnections with cell edges or ligaments, closed cells arrangements display mostly isolated cells by solid faces. These characteristics can be assessed from the foam permeability to a fluid or by optical microscope.

Open cell metallic foams allow the passage of fluids, being used for different applications, from filtering extending to heat exchange. Closed cell configuration is optimal for energy absorption and structural applications. For the matters of this work, the specimen in study, UniPore, presents an open cell structure.

2.2 Manufacturing processes

As defined, there are many different classifications of cellular materials. For each classification, there are several types of manufacturing processes capable of producing these structures. The elaborate internal geometry of a cellular structure makes the manufacturing process difficult with traditional means of machining. As such, researchers have looked to other technologies like additive manufacturing, moulding, forming, and joining as possible production means for this kind of materials. [10, 8]

The pores random distribution in stochastic cellular materials is connected with the manufacturing process, typically by introducing a bubbling agent to metal during a

solidification transition. Whereas ordered cellular structures have careful manufacturing processes, being more difficult and expensive than the ones for disordered structures. [5]

Contrasting with traditional manufacturing technologies additive manufacturing (AM) create parts through the successive addition of material layer-by-layer, while the firsts work by removing material from a work piece until getting the desired geometry. The layer-by-layer nature of AM processes supports the conception of complex geometries that cannot be fabricated by other means. [14, 15, 10]

Besides this technologies based on additive manufacturing there are progresses in producing cellular materials with a certain degree of organization by means of explosive welding. Explosion welding is a solid-state metal-joining process that uses explosive force to create an electron-sharing metallurgical bond between two metal components without an appreciable temperature increase in the metals. [16]

In explosion welding exceptionally high pressures are utilized to join metals. As the materials do not melt, two metals with considerably different melting points can be effectively welded by explosion welding. Regarding this circumstance, one can anticipate that, joining metal to produce a cellular material will not change significantly the metal chemical structure. The force and speed of the explosion are directed to cause a series of progressive shock waves that deform the faying surfaces at the moment of impact. A magnified section of the joint reveals a true weld with an interlocking wave shape. [16, 17]

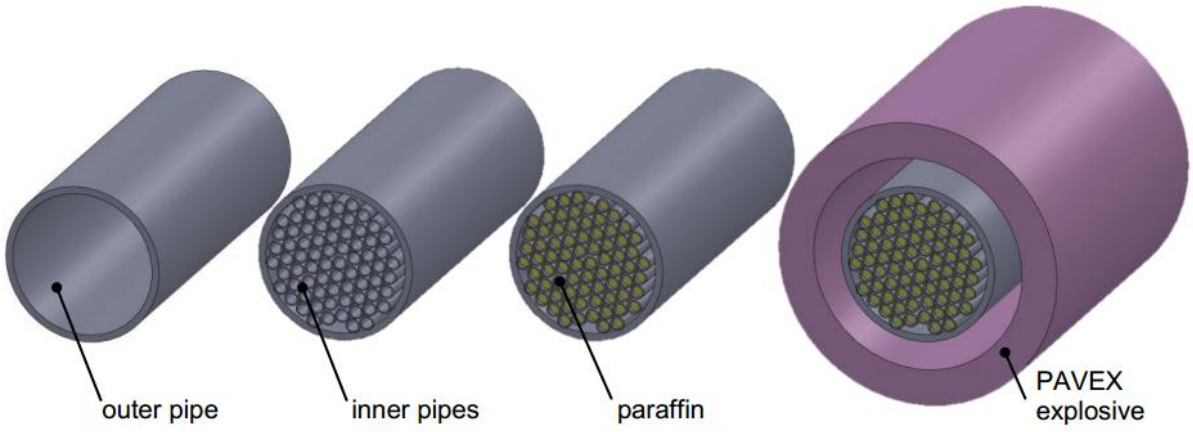

Figure 2.3 - Explosive welding procedure for UniPore manufacturing. [17]

2.3 Properties

Cellular solids have physical, mechanical and thermal properties which are measured by the same methods as those used for fully dense solids. Both physical and mechanical properties of the foams are affected by relative density, morphology and size of the pores. These characteristics are, as well, influenced by the processing methods. [7]

2.3.1 Density

The relative density is a preponderant characteristic which affects foams mechanical properties. It is known that as the relative density increases, the cell walls become thicker and the pore space decreases. This important structural characteristic, relative density, ρ_r, which characterizes a cellular solid is then calculated by the Equation 2.1,

$$\rho_r = \rho^* / \rho_s \tag{2.1}$$

with ρ^* being the density of the cellular material and ρ_s the density of the solid material which composes the walls.

The fraction of pore space in the foam is called porosity, it is in fact

$$p = 1 - \rho_r \tag{2.2}$$

Typically, cellular solids have relative densities, which are less than approximately 0.3. Often considerably less dense cellular materials can be found – with relative density as low as 0.003.

2.3.2 Structural properties

There are numerous structural parameters to provide characterization of cellular metallic materials, that is to say geometry and shape of the pores, number, average size and size-pore distribution, thickness, among others. Most mechanical properties depend slightly on cell size, usually, cell shape is more significant. If the cells have equal geometry properties they are isotropic, but if the cells are even slightly elongated or flattened the properties will be heavily dependent on direction. [7]

Other important geometric aspect of cell structure is anisotropy, the tendency for cells to have unequal wall thickness, to be elongated or flattened. The connectivity between edges and faces, the number of contact neighbours vary from structure to structure and may significantly influence properties as well.

Cellular metals are heterogeneous materials since the pores are inserted in the metal cell frame. The description of cellular materials presents itself as an intricate task and, as a consequence, no general rules for the characterization of cellular metals have been established. [8]

2.3.4 Mechanical properties

The undertaken literature studies on mechanical properties of metal foams have been providing understanding on the mechanical behaviour of a wide range of cellular solids. Gibson and Ashby have presented an extensive investigation on this referred field.

Both static and dynamic compression tests have been a tool to assess mechanical properties of metallic foams. The typical testing apparatus operates with hydraulic pneumatic or servo-mechanical power to compress or extend the specimen.

Dynamic testing is implemented to determine the behaviour of materials at high strain rates such as when designing for crash or blast loadings. Static tests, with a strain rate inferior to $10^{-1}\ s^{-1}$ are used to study foam properties such as deformation under compressive loads, elastic deformation, collapse, plateau stress and energy absorption. The significant properties obtained from static tests are the elastic modulus, yield strength, plateau strength and the absorbed energy at a certain stress or strain. [1]

2.3.4.1 Stress-strain behaviour under compression

It is stated that cellular materials can go through large deformations when subjected to compressive loading. Under compressive loading cellular materials have a characteristic stress-strain correlation that can be divided into four main areas: [18]

i. quasi-linear elastic response,
ii. transition zone, where the cellular materials first exhibit buckling, plastic deformation and collapse of intercellular walls,
iii. stress plateau, where the mechanism of buckling and collapse becomes even more evident, arising in large strains at almost constant stress and
iv. densification, where the cellular material stiffness increases and consequently converges towards the stiffness of the base material.

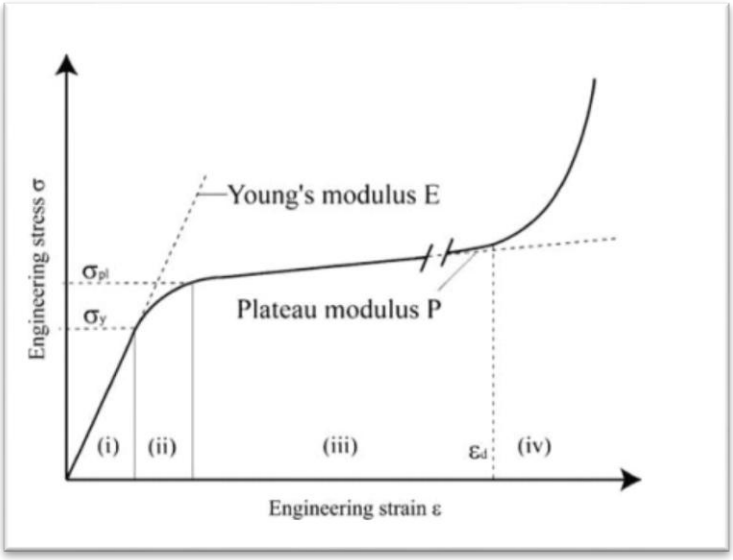

Figure 2.4 - Cellular materials characteristic compressive behaviour representation [18]

Significant parameters like the elastic modulus, the plateau stress and the densification strain may be determined with the help of these curves. The referred parameters increase with the growing of the density, whereas the defects or imperfections have unfavourable effects on the mechanical properties. Similarly, compressive stress behaviour increases with increasing the foam density.

Linear elastic region the first region of the stress strain curve is the linear elastic region in which the stress increases practically linearly with the strain. The deformation in this region is controlled by cell wall bending or stretching, depending on the

open or closed cell structure of the foams. Open cell constructions of low relative density present deformations predominantly by cell wall bending. For increasing relative densities, ($\rho^*/\rho_s > 0.1$), cell edge compression plays an important part. In addition, the thin membranes of the closed cell architecture that creates the cell faces, stretch normal to the compression axis, contributing to the modulus. In the open cell geometry case, if the strain rate is unusually high, the fluid flow affects the elastic module. [7, 9, 19]

Simple cubic unit cell model was developed by Gibson and Ashby in order to predict the normalized mechanical properties of the foams. Despite the simplified version of cell walls, the cubic model allows for a useful understanding of deformation and failure mechanisms.

There are other several models to predict the elastic modulus, which is a significant parameter to be determined in this region.

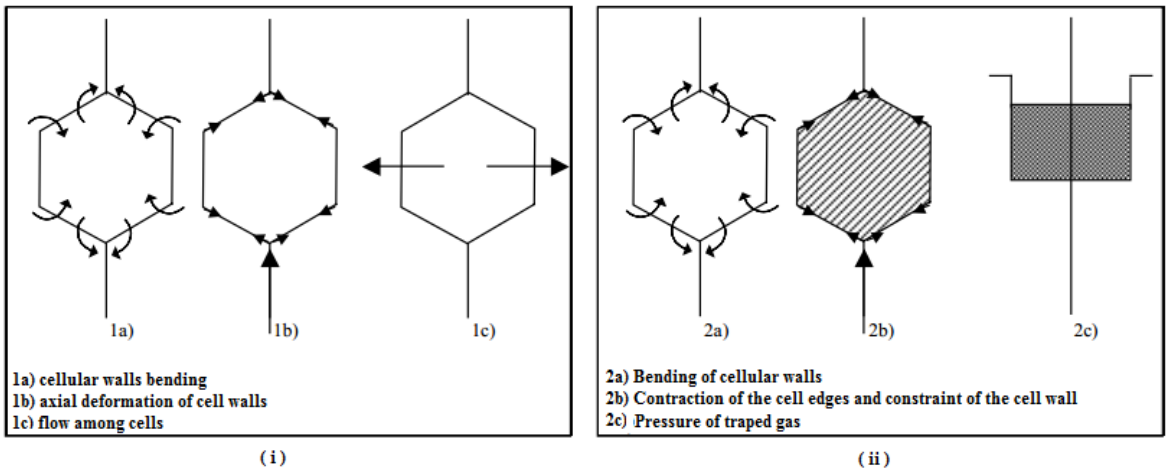

Figure 2.5 - Deformation Mechanism in foams, (i) open cells foams and (ii) closed cells foams [19]

Based on the referred unit cell model, Gibson and Ashby proposed the following equation of the elastic modulus of the open cell foams (E*) which is calculated from the linear elastic deflection of a beam with length l, loaded at its mid-point by a load F:

$$\frac{E^*}{E_s} = C_1 \frac{\rho^*}{\rho_s} \tag{2.3}$$

Where ρ^* represents the mass density of the cellular material, E_s and ρ_s the Young's modulus and density of the solid structure, respectively, and C_1 is a constant that needs to be determined by experimental fitting. Nonetheless, experimental elastic modulus of open cell foams showed that the constant C_1, is closely equal to the unit.

Young modulus is dependent mostly on the foam density, where the last will increase with the rise of the density.

Plateau region Failure region continues with a stress plateau either with a constant value or increasing slowly with strain. Linear elasticity is generally limited to small strains. In this area, the deformation is possible to recuperate although nonlinear. Foams made

from materials that have a yield point such as rigid as polymers or ductile metals collapse plastically when loaded beyond the linear elastic region. Numerous deformation mechanisms occur in this area, namely elastic buckling or brittle crushing of the cell walls and formation of plastic hinges. Plastic collapse results in a long horizontal plateau in the stress strain curve, analogous to the elastic buckling, however, the strain is no longer recoverable.

The plateau tension (σ_{pl}) is determined with regards to the beginning of the plateau region, where the plastic regime begins. [1, 19]

Densification region succeeding the plateau region, at a critical strain, the cell walls start to have contact between themselves and the densification region begins. The stress in this region increases rapidly and approaches to the strength of the solid foam material. Foam densification occurs at the densification strain ε_D , the point where the foam starts densification diverges among researchers. Visual inspection presents itself as common method to determine densification strain or stress. Other method utilizes the point of intersection of the slope of the plateau region and the point of densification, located in the densification region. In structural applications, this densification point is not as significant as the yield point. On the other hand, for energy absorption purposes, the densification point is fundamental, and compression beyond densification should be avoided due to the severe increase in stress. Densification strain, as well, decreases with increasing relative density. [1, 2, 20]

Reviewing, the useful properties of cellular solids depend mostly on the material from which they are made, the relative density, and the intern geometrical structure. It is important to link the physical properties of cellular solids to the corresponding density and complex microstructure, in order to understand by what method such properties can be optimized for a given application. The structure, size, shape and topology of cells represent a great influence on the characterization of cellular materials.

2.4 Cellular Materials Applications

Depending on the class of cellular structure, open or closed cell metallic foams have a large variety of industrial applications, furthermore, the size of cellular pores is desirable to be adjustable according to the intended application. In general terms, some aspects are assumed

- Morphology: architecture of the pore (open or closed), porosity, total internal surface area;
- Metallurgy: chemical composition of metal or alloy or base material microstructure;
- Processing: manufacturing availability regarding the geometry, component dimensions
- Economy: cost issues, appropriateness for large volume production. [9, 21]

Structural, load bearing parts have to be light because otherwise they would be made from conventional massive metals or alloys. To simplify one can distribute applications to a form of gradient from ‘‘functional’’ to ‘‘structural’’. Answering from which metals or alloys a given type of cellular structure can be manufactured is likewise important.

Aerospace, automotive, and defence industries would largely benefit from the creation of components produced with cellular materials. The remarkable characteristics of these materials would make them successful in several types of structural component, offering gains in weight without compromising strength. The reduced mass of these materials would benefit applications that require low moments of inertia, such as arms for industrial robots. [10] The material's capacity to absorb impact could be used for light-weight armoured reinforcement on military vehicles, or as effective shock absorbers on automobiles.

The largest limitation of stochastic cellular structures is the complete lack of control that a designer has over the topology of the mesostructure. Example applications of designed cellular mesostructure take account of a jet engine combustor liner that has the necessary strength to endure extreme pressures and stresses from thermal expansion while still maintaining open cells that allow for active cooling via forced convection (Figure 2.6 a) and a lightweight blast resistant panel that efficiently absorbs impact from large impulse forces (Figure 2.6 b). [22, 23]

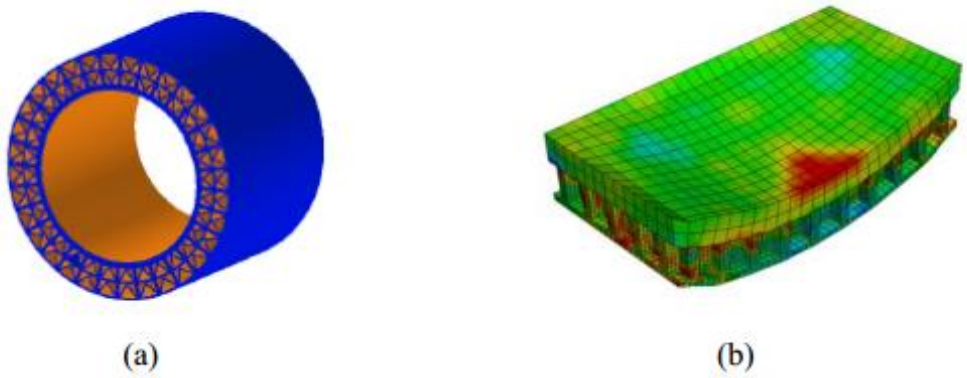

Figure 2.6 - Cellular structures with ordered architecture application examples.

In addition, cost issues are preponderant to plan for industrial application. Accounting for the material feasibility or processing method at a reasonable price is vital. [9]

2.5 UniPore Material

The UniPore material is manufactured through blast loading welding. The loading in the object caused by the air blast from an explosion striking and flowing around the object is a combination of overpressure and dynamic pressure loading.

The explosion welding has a marked interest since welding operations can be carried out quickly, reliably and without being dependent on external energy sources, such electricity or gas. UniPore, as other explosion welded products, do not exhibit many of the metallurgical characteristics of fusion-welded, brazed, or forged products. The process is an effective joining method for virtually any combination of metals with only sufficient ductility and fracture toughness to undergo rapid deformation without fracture being the metallurgical

limitations. Foremost products manufactured by this process are large clad plates used in pressure vessels, heat exchangers, and electrochemical process applications. [24, 22]

As it may be verified in Figure 2.7, UniPore material is composed by unidirectional pores. This is a result of the tight alignment of small diameter thin walled pipes, which are welded along the contact surfaces during the blast loading of the outer pipe with a larger diameter. The small diameter tubes are filled with paraffin in order to preserve the geometry as much as possible throughout the manufacturing process.

The sample illustrated in Figure 2.7 was the basis for a CATIA three-dimensional model and, posteriorly, for the computational model. As a result, the overall dimension and other conditions like the arrangement and thickness of the walls are an approximation.

The manufactured sample has a diameter, *D*, of 30 mm as well as 30 mm length, *L*, and its base material is copper.

Copper become stronger and more ductile as temperature goes down. They also retain excellent impact resistance among other desirable properties in what concerns to engineering applications. Further mechanical information, relevant for the study will be displayed in Computational section, specifically in Table 3.1.

Particularly, the sample presented in Figure 2.7 was manufactured in phosphorous deoxidized copper. This copper is produced by adding small amounts of deoxidizing agents, typically phosphorus, to remove oxygen from melt. Although possible, deoxidized coppers are generally not used for electrical applications. Applications for these deoxidized coppers vary from industrial to automotive passing through building or plumbing. Corrosion resistance along with thermal and electrical conductivity is some of the main motives for the mentioned applications. [25]

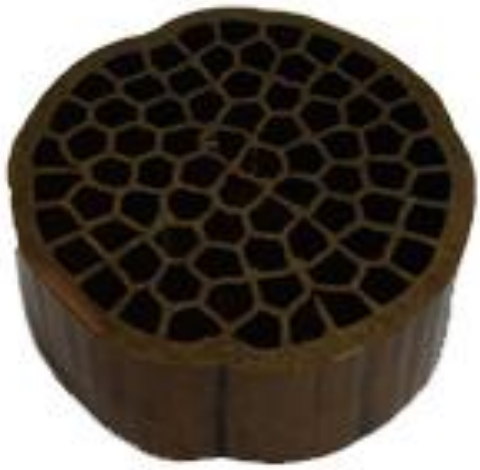

Figure 2.7 - Aspect of UniPore material, manufactured by compressive blast loading

3. COMPUTATIONAL MODEL – UNIPORE MATERIAL

The finite element method allows for accurate predictions reducing costly experimentation, thus achieving economical yet accurate designs before testing real prototypes. [21]

Being UniPore a new material, and, as almost no physical tests were performed, the computational simulation will give information to explore the adequate geometrical parameters without spending resources in experimental essays.

Finite element analysis comprises pre-processing, solution and post-processing phases, the following sections will be presented in this same order. The finite element procedure is based upon some assumptions in order to approach the real case-study problem to the mathematical model. A suitable model definition for the material behaviour undertakes a primary role to obtain reasonable results. Some mechanical and physical properties must be known in order to establish the mentioned model. This definition step precedes the analysis and calculus of the problem.

Briefly, the Finite Element analysis takes several distinct phases:

1. geometrical modelling of the examined real problem
2. assigning materials and their properties;
3. definition of system loads;
4. definition of boundary conditions;
5. generation of the finite element mesh;
6. numerical calculations;
7. visualization and analysis of results.

The Finite Element (FE) Analysis simulates the actual compression tests by performing a linear analysis of the specimen under both uniform transversal (Figure 3.1, a) and longitudinal compression, (Figure 3.1 b) as well as a nonlinear analysis under transversal compression.

The FE analysis was performed using the FE package ABAQUS®. First, a geometric model of the specimen was created using the software CATIA®. This bi-dimensional model was, afterwards, imported to ABAQUS® pre-processor. In the next stage, the material model was extruded into a three-dimensional model.

Properties of the structural components of the specimen were defined according to the desired testing; first copper, after aluminium and finally carbon steel. The necessary properties were introduced in ABAQUS®.

The finite element model was constructed from the three-dimensional exemplar by meshing the surfaces of the geometrical model to create nodes and elements. Shell finite elements were used. Shell elements are used to model structures in which one dimension, the thickness, is significantly smaller than the other dimensions; therefore these elements are a suitable option, based on the cellular structure geometry.

Reduced integration releases computing effort but can also lead to mistakes and this is the reason for using hourglass control, in order to prevent possible errors.

The boundary constraints that would simulate the conditions of each actual compression test were defined. With this information, the input file was generated and the analysis was accomplished using ABAQUS®. The aforementioned steps are illustrated and clarified in the next section for each compressive state.

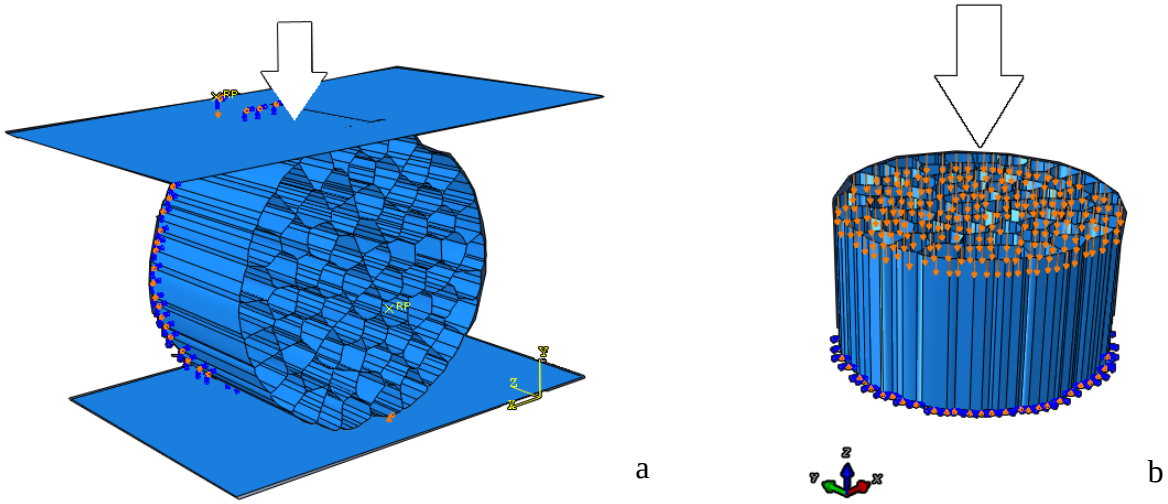

Figure 3.1 - Compressive loading conditions a) transversal and b) longitudinal

3.1 Computational Models

For the current purposes, it is appropriate to state that a computational model is a set of computational codes, executable in a specific software environment that modifies a group of input data into a set of output data. This data, introduced, transformed and generated in the process, generally has interpretation in real-world terms. [26]

This chapter contains the adopted procedure to accomplish the computational study as well as a brief description of each model. The models were submitted into a numeric linear analysis in order to determine the Young's modulus of the cellular structure.

The use of specimens having large L/D ratios should be avoided to prevent buckling and shearing modes of deformation, therefore the study will consider a cylindrical specimen with outer diameter 30mm and equal length, under outer force loading transverse and longitudinal direction in relation to the sample cross-section, which may be clarified in Figure 3.1.

A highly refined mesh implies extensive computational time and increases the chance of miscalculation due to the large number of elements. Although the considered model has 30mm length, the specimen used in the analysis is 15mm length. A symmetric boundary condition was applied, hence the number of elements decreased in half.

In order to define the ideal mesh size it is necessary to perform a convergence study on the mesh size. In this stage, the displacement is the supervised variable, when the result analytically converges to a value, it can be assumed that a suitable mesh was achieved. This mesh size will be used in the subsequent analysis ensuring results with required reliability.

Summarizing, the basic characteristics of the computational model and as a result of the mentioned conditions, the analysis was accomplished using quadrilateral shell finite element with four nodes. These elements correspond to the linear geometric type. A structured mesh was used.

3.2 Computational Modelling

In the following section, there will be an introduction on the computational model used to perform the analysis. This real model has irregular structure due to the process used to fabricate it.

Therefore, the appropriate computational model involved the creation of a geometric model that would closely represent the irregular shape and dimensions of the test specimen. (Figure 3.2)

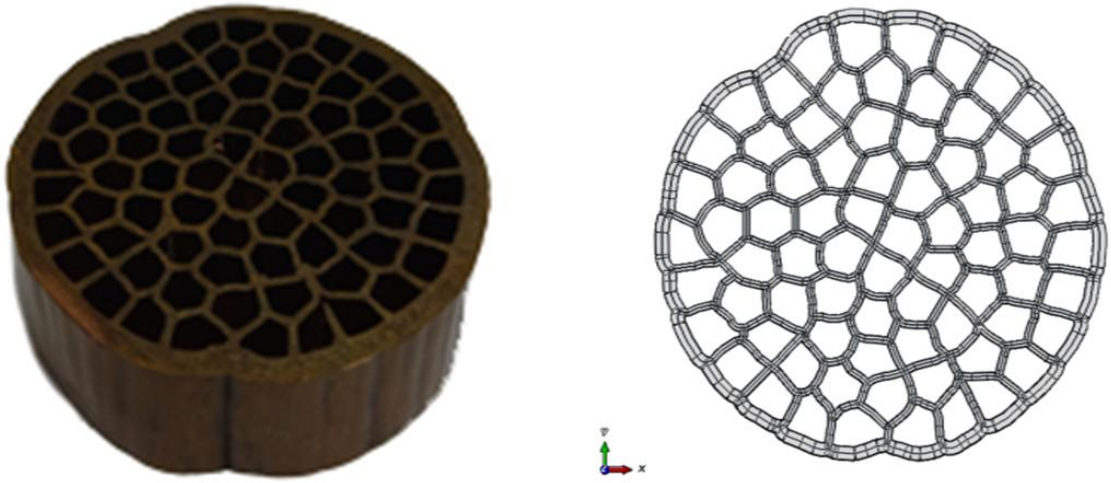

Figure 3.2 – Physical UniPore material sample (left) and render of shell thickness applying scale factor 0.2, XY plane view (right).

The geometrical model imported to ABAQUS® (Figure 3.2), and therefore the one submitted into analysis, is an approximation of mid-side surfaces (walls). This sample was designed in order to perform a shell element analysis. This way the characteristic thickness variation within the walls was not taken into account for this model. Once the model was designed using the mean distance among each cell wall to draw the middle line, it is possible to obtain a good reproduction of the real model, with constant thickness walls.

In the property selection step, two different sections were assigned for the walls as it is shown in Figure 3.2. These two different section assignments correspond to the outer wall of the specimen, which is ticker then the inner wall, associated with the former assignment.

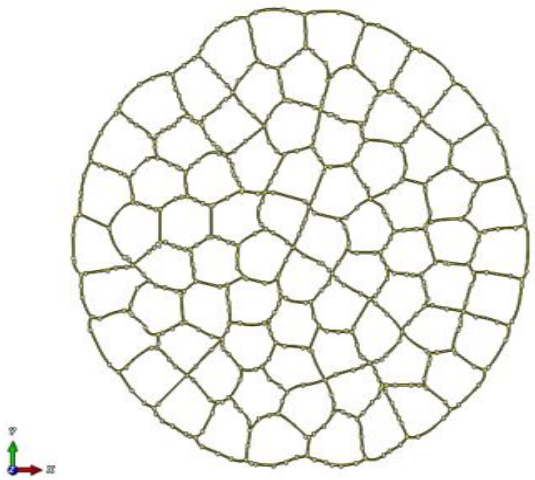

Figure 3.3 - Computational model before extrusion

The base material of the specimen will be assigned first as copper, then as aluminium and, finally, as steel. For these materials, the performed analysis will consider the elastic behaviour. The input values for each material are presented in Table 3.1. However, in this elastic analysis the information on the Young's moduli as well as the Poisson's ratio are the only values to add as mechanical properties.

Table 3.1 – Base material properties [27]

	unit	Copper	Phosphorous deoxidized copper	Aluminium (6000 Series)	Steel (low carbon series)
Density	kg/m^3	8930	8930	2700	7870
Young's modulus	MPa	110 000	110 000	689 00	200 000
Poisson's ratio	-	0.343	0.364	0.33	0.29
Yield stress	MPa	33	333	276	415
Tensile strength	MPa	210	344	310	540
Elongation at break	%	60	20	10	10

The development of the FE model involved meshing the surfaces of the geometric model with quad-dominated structured 4-node shell elements, with reduced integration, hourglass control and finite membrane strains.

After the definition of the geometry, the subsequent step is prescribing the boundary conditions. The conditions are dependent on the type of compression that the specimen is subjected to, for that reason each longitudinal and transversal compression will be regarded separately in the subsequent section.

3.3 Computational simulations

Overtaken the stages of configuration and definition of the geometry of the problem, as well as the circumstances to which it is subjected, the simulation arises as the next step from which are extracted the results, values that will later be submitted to a detailed analysis.

Bearing the disadvantage of porous material being irregular and inhomogeneous the procedure will ensure the test of different cell sizes, in irregular models. As this production method allows a relative cell size control is relevant to inquire the geometry that fulfils the demands of this new material requests. There will be a variation in both inner (t) and outer (T) wall thickness, respectively: t = 0.2, 0.4, 0.6mm and T = 1.0, 1.5, 2.0mm with perfectly straight aligned pores.

In what concerns to the longitudinal analysis and having as support the computational values obtained for stress strain parameters, it was initially attempted to determine the values for the Young's modulus associated with the linear area.

Regarding the transversal analysis, the attempted deformation was 1% as well for the linear analysis. For the elastic region, increasing deformations were empirically attempted until achieving 8.3% of deformation. This value relates to the transition zone, where the cellular materials start having plastic deformation, which means that, for a displacement of $\Delta = 2.5\text{mm}$ the quasi-linear elastic response ends, and the material reaches its yield stress, at this point begins the stress plateau.

In the following sections, results of finite element analyses will be presented, the calculations were performed using the commercial package ABAQUS®, within the finite strain formulation of incremental plasticity which is standard in this software.

Convergence was verified by increasing the number of elements in the mesh for several representative runs and verifying that the results did not change significantly.

3.3.1 Model Simulation

The verification of the model is an important procedure that ought to be conducted for any FE analysis. The verification was performed for both transversal and longitudinal compression model once there are significant differences among these models, therefore both require convergence analysis.

The reason for performing a convergence study on the mesh size is linked with the commitment between acceptable computational efforts and accurate results. A mesh can be considered to be dense enough when the displacement does not change significantly with the increasing number of elements.

This way, several attempts for each simulation were taken, according to the stipulated procedure. The value taken for longitudinal displacement in Z direction, as it is possible to

confirm in the previous section for boundary conditions was $\Delta l = 0.15$ mm which corresponds to $\varepsilon = 1\%$ of displacement for the longitudinal model.

The size of the finite elements was decreased with small intervals, fluctuating between [1.6 and 0.16] mm. The displacement of a centrally positioned node was observed and each value obtained corresponded to 0.15 mm in negative Y direction, the main direction for the matter of this analysis. The ratio achieved for the reference value was unitary for all size elements once the displacement did not changed with the elements size.

For the longitudinal model, there was no substantial difference between results with coarse or refined mesh variation. The displacement followed had always the value of 0.15 mm and the percentage difference among displacements resulted in a ratio with the value 1, as predictable. For this longitudinal analysis was concluded that the inner wall geometry of the model does not represent a preponderant role in the stiffness of UniPore material. However, the cross-section area is of crucial importance.

For the transversal model, the value prescribed in the boundary condition for displacement was $\Delta l = 0.3$ mm this corresponds, once more, to $\varepsilon = 1\%$ in the global model.

Table 3.2 - Value for displacement in the central node of the model and respective ratio for the reference value.

Number of elements	Finite element size [mm]	Displacement U2 [mm]	Percentage difference
6399	1.6	0.119182	0.903715
8688	1.3	0.119243	0.904178
11340	1	0.12874	0.97619
12654	0.9	0.128803	0.976668
19140	0.675	0.128962	0.977874
29290	0.51	0.128865	0.977138
50076	0.38	0.130812	0.991902
88440	0.28	0.13188	-

According to the results in Table 3.2, the optimal mesh would have 0.28 mm mesh size, with which was possible to achieve the most accurate result. According to the data in Figure 3.4, the axial model could include the essays displayed in red colour dots. However, the acceptable mesh is 1 mm size, which allowed the desired convergence. This way, the convergence process is represented in the diagram of Figure 3.4.

Regarding the mesh size, displayed in Figure 3.5, composed of 11342 elements, once the results of mesh convergence were achieved and the mesh size defined, the preparation of the models boundary conditions and loads was the following step.

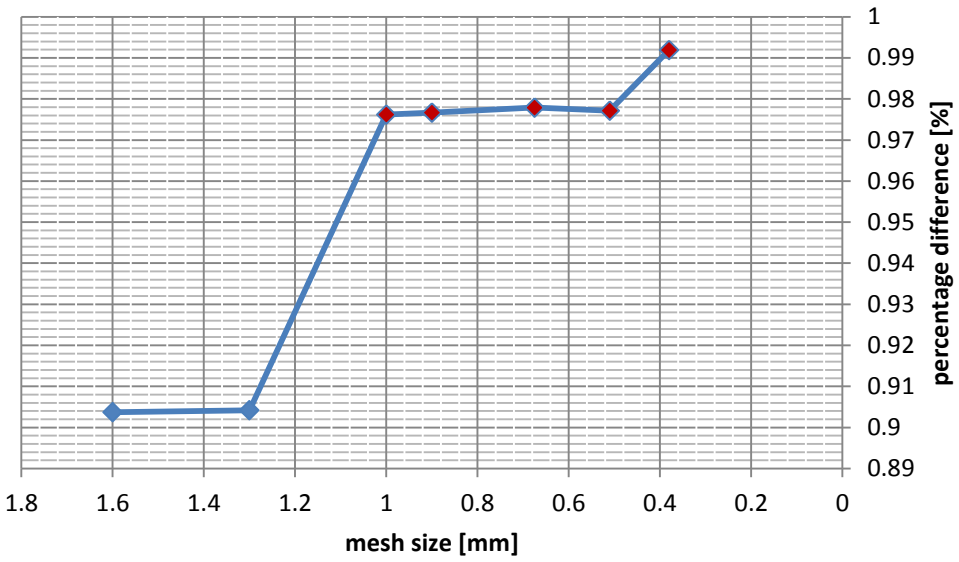

Figure 3.4 - Displacement ratio for each mesh size.

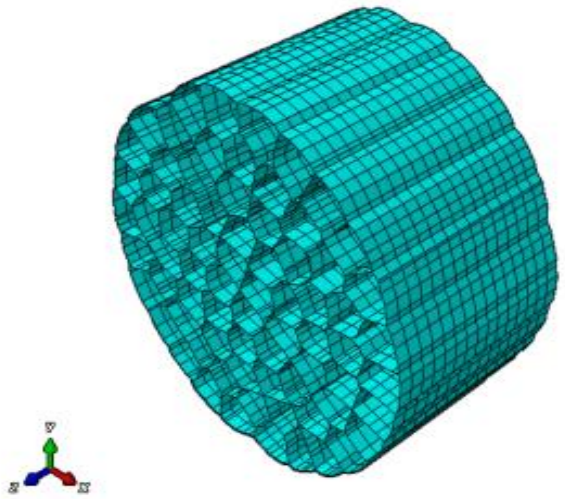

Figure 3.5 - Illustration of the optimal mesh obtained (1mm size, 11342 elements).

3.3.2 Boundary Conditions for longitudinal compression

The bottom of the model was set to feature the symmetry condition, as shown in Figure 3.6 (represented with yellow colour), as already mentioned. This circumstance relies exclusively on decreasing the number of finite elements to half and, as a result the computational model becomes faster.

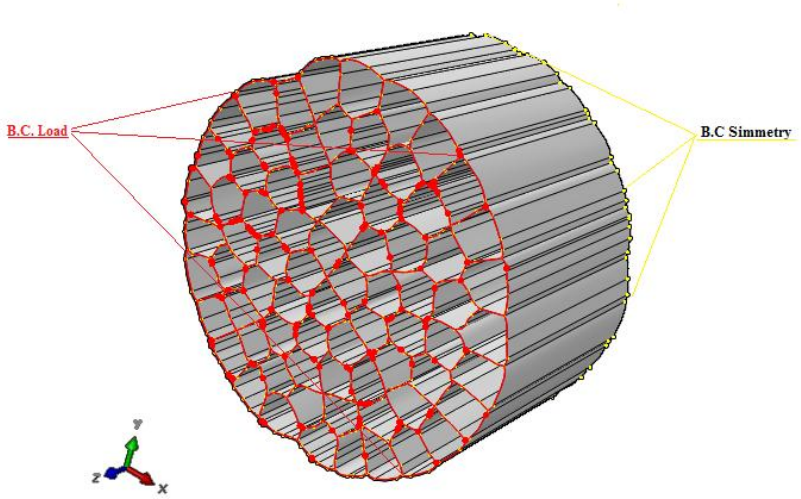

Figure 3.6 - Lines where was applied the boundary condition for symmetry (bottom – yellow), and for the load (top – red), isometric view.

The fixation of the bottom point as presented in Figure 3.7 intends to simulate the actual contacts between the specimen and the essay device. This way, all the displacements and rotations for X, Y and Z directions were set as U1=U2=U3=UR1=UR2=UR3= 0.

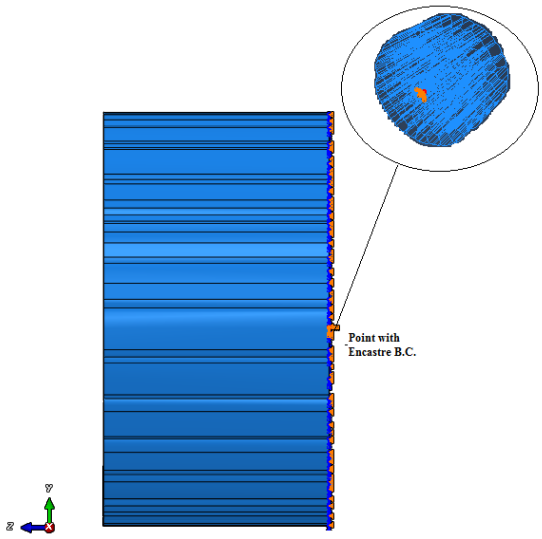

Figure 3.7 - Boundary condition: *Encastre*, ZY plane view, with detail of location (bottom) in the model with isometric view.

Finally, the displacement was applied, which describes the displacement experienced by the specimen when undergoing the real compression. This value was primarily set in order to obtain $\varepsilon = 1\%$, the value for displacement was $\Delta l = 0.15$ mm in the negative direction of Z-axis, since it was a compression test (Figure 3.8).

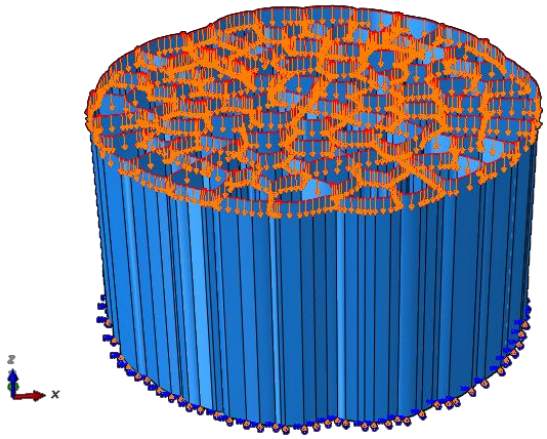

Figure 3.8 - Applied displacement (orange arrows), U3=-0.15mm; isometric view

3.3.3 Boundary Conditions for transverse compression

The model used in this compression test comprises the specimen along with two rigid shell homogeneous plates sufficiently large to compress the specimen in all its extension.

The specimen compressive test in the transverse direction was taken under the four boundary conditions described below. The number of increments was automatically calculated by the software for each test.

The symmetry condition remained in the model for transverse compression, this time, with the adequate changes: U3=UR1=UR2=0. Hence, is implied that the specimen, contained between two rigid plates, is yet again, symmetric in the Z direction. With this boundary condition application the size was diminished to 15mm width, in consort with 30 mm height.

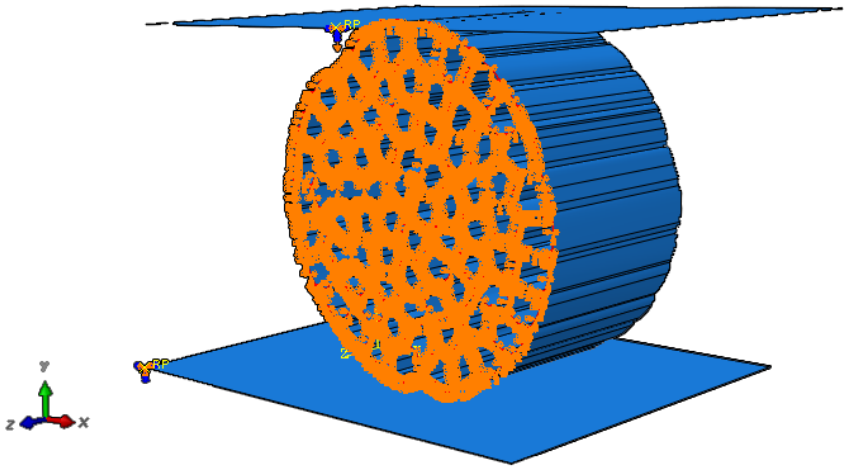

Figure 3.11 - Boundary condition for symmetry, isometric view

As the specimen is, in this instance, between two plates, there will be a propensity for the specimen to slide along the X direction side. In order to recreate the real essay, where the

friction between the plates and the sample will contend the sliding, a fixation for displacement

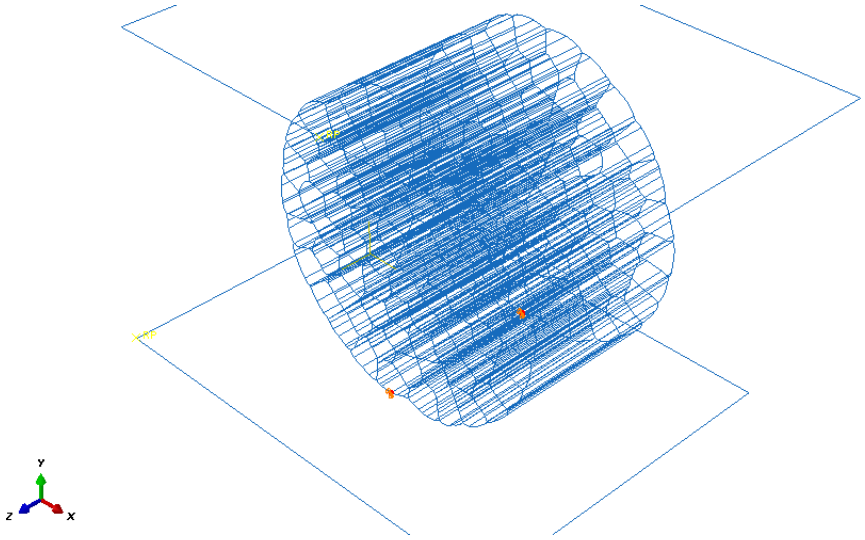

Figure 3.9 - Detail of nodes with fixation U1=U2=0.

both in X or Y direction, was applied in two specific nodes, where U1=U2=0, Figure 3.9. Therefore is assured that the nodes in contact with the plate surface would not move in other direction than the Z direction, allowing the specimen to expand in that direction when under compression. For the upper plate, such boundary condition was unnecessary once for the interaction contact was applied a friction coefficient as it will be addressed under the respective sub-section.

The plates presented in the illustrations for transverse compression were, each, prescribed with a boundary condition. These conditions were applied to a Reference Point (RP), illustrated in figures as RP, in yellow colour. For both rigid plates the boundary conditions considered that no displacement or rotation was allowed, exception made for the upper plate where Y direction (U2) was variable, assuring the displacement of the upper plate. To the point, the bottom plate was set with zero displacement or rotation: U1=U2=U3=UR1=UR2=UR3=0. In addition, the upper plate was first set for displacement U2=-0.3 mm (corresponding to $\varepsilon = 1\%$) and U1=U3=UR1=UR2=UR3=0 assuring that the specimen would suffer a pressure rigorously under Y direction; this is to say a pressure normal to the cross-sectional area.

3.3.3.1 Interactions

As a consequence for having two rigid plates, and in order to correspond with the real case scenario, it was deliberated that the interaction properties between the two plates and the specimen should be distinct. The interaction surfaces between each plate and the specimen may be identified in Figure 3.10. In this surface-to-surface contact the slave is the specimen and the master surface is the plate. In the stipulated node-to-surface discretization method the tie coefficients were set equal to the coefficients of the interpolation function, at the point where the slave node is projected onto the master surface. This means, that multiple master nodes have to be used. The master surface was smoothed 0.2 times and the slave surface was adjusted only to remove over-closure.

After the boundary conditions were defined for this axial compression with two different parts (the rigid plates) in contact with the model, was necessary to define interactions among the plates and the specimen.

Both bottom and upper plates were defined with different contact properties. Bottom plate has a tangential behaviour with frictionless contact and the upper plate has a tangential behaviour with a friction coefficient, $\mu = 0.3$, the recommended value for this contact type [28].

The interactions were defined with the intention of reproducing the contacts that would occur between the plate and the specimen upon the real mechanical loading. The surfaces assigned for contact were picked taking into consideration the fact that, at small strains, the model would be deformed mostly in the contact between the plates. Once the displacement is controlled by applying a load in the upper plate, larger deformations are expected for this region.

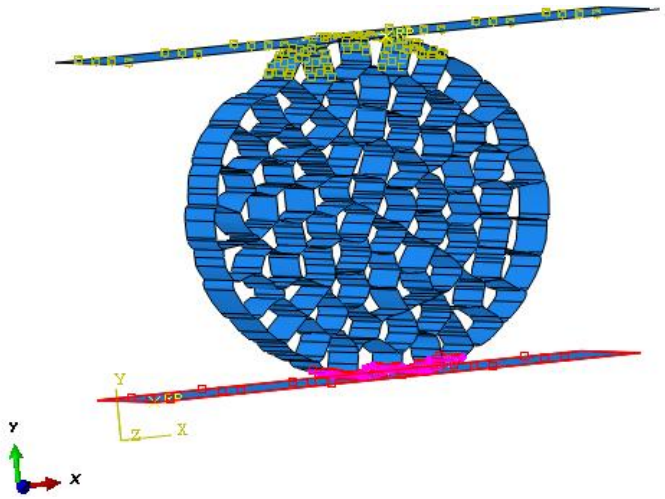

Figure 3.10 - Interactions between specimen and bottom (magenta) and with upper plate (yellow).

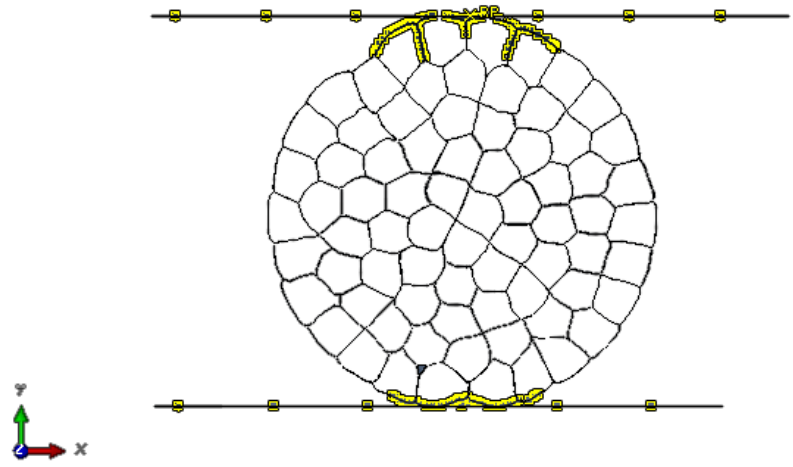

Figure 3.11 - Prescribed contact interactions between specimen and plates, in yellow appointed surfaces for interaction

4. RESULTS AND DISCUSSION

As a part of this study, the effective Young's modulus was evaluated as well as the reaction force variation within the thickness of the walls. The stress-strain diagram was determined for evaluation of the variation of the parameters.

At small strains ($< 10^{-3}$), metals behave like linear elastic solids. An applied stress simply stretches the atomic bonds and Young's modulus which measures their stiffness, is usually large. [7]

The engineering measures of stress and strain, under unidirectional force, denoted here as σ_e and ϵ_e respectively, are frequently described by the simple mathematical expression using the original specimen cross-sectional area A_0 and length L_0 as in the following expressions

$$\sigma_e = \frac{F}{A_0} \tag{4.1}$$

$$\epsilon_e = \frac{\Delta L}{L_0} \tag{4.2}$$

where *F* is the applied force, *A* the area and *E*, Young's modulus.

After performing the longitudinal compression analysis of the model with ABAQUS®, the reactions observed in the plot for each increment, i were summed up. The results characterize the reaction forces at the bottom plate of the model by adding the resultant reaction forces RF.

According to equation 4.3 was determined the engineering stress:

$$\sigma_i = \frac{RF_i}{A} \tag{4.3}$$

where A is the total area of the projection in the surface model in the direction of displacement, Table 4.1. For the transversal model the area was calculated with the expression $A = l \times d$, where l is the length of the specimen, and d is the diameter. For the longitudinal model, this area value was gathered from CATIA® *information tool*. In the last, there is a distinction for the projected area of the whole model, named solely as projected area and the projected area without voids, entitled walls projected area, which means the solid part of UniPore. This information is complemented by Figure 4.1.

Table 4.1 - Projected area values used to obtain the engineering stresses

	Longitudinal compression	Transversal compression
Projected area, A [mm^2]	664.8	900
Walls projected area [mm^2]	258.459	-

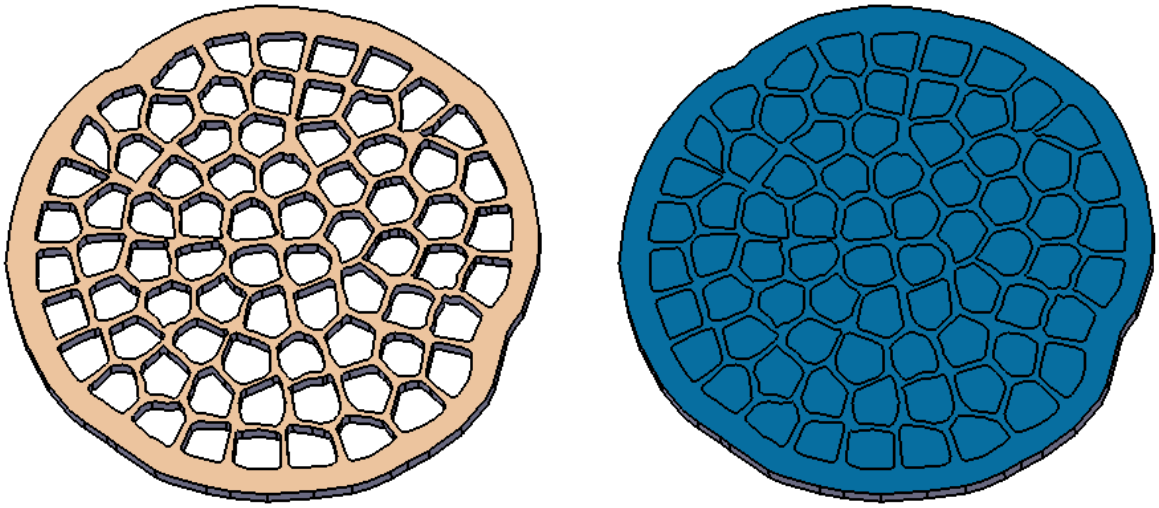

Figure 4.1 - Projected areas for longitudinal compression, walls projected area in light orange, 258.459 mm^2 and whole specimen projected area, in blue, 664.8 mm^2.

Using equation 4.4, the deformation of the material was calculated for each increment as well:

$$\varepsilon_i = \frac{\Delta l_i}{l} \tag{4.4}$$

where Δl_i is the length variation, calculated by multiplying time increment and the displacement imposed in the boundary condition. Finally, l is the original length in displacement direction.

The parameter that quantifies elasticity, Young's modulus which absolute value can be determined by the Hooke's relation:

$$\sigma = \mathrm{E}\,\varepsilon \tag{4.5}$$

This calculation associated with the linear region, with an approximate deformation of 8.3%. For this purpose was enough to make the stress with the respective strain value, defining Young's modulus by Hooke's law.

The engineering stress-strain curve must be interpreted with caution beyond the elastic limit [29], since the specimen dimensions experience considerable change from their original values. Using the true stress $\sigma_t = \frac{F}{A}$ rather than the engineering stress $\sigma_e = \frac{F}{A_0}$ can give a more direct measure of the material's response in the plastic flow range.

$$\sigma_t = \frac{F}{A}, \quad \epsilon_t = ln\frac{L}{L_0} \tag{4.6}$$

As mentioned in the introductory chapter porosity is a preponderant feature for cellular materials. This way, using equation 2.1 as well as 2.2 for the specimen with outer wall 4mm and inner wall 2mm comes:

$$\text{Porosity} = \frac{A_{void}}{A_{Total}} = \frac{4.0634 \times 10^{-4}}{6.648 \times 10^{-4}} = 0.6112$$

The values for A_{VOID} and A_{TOTAL} were acquired in CATIA® software.

From equation 2.2:

$$0.6112 = 1 - \rho_r \Leftrightarrow \rho_r = 0.388$$

The relative density of UniPore manufactured sample is, then 0.388. This value will vary according to the wall thickness reproduced in the computational model. Results related with thickness variation will be presented in the referred section once it is considered relevant to observe the values together with the remaining results.

4.1 Linear Analysis

4.1.1 Longitudinal compression

In order to infer associations, the elasticity modulus progression was evaluated for every material: aluminium alloy, copper and carbon steel. The finite element global mesh is 1 mm size and the first numerical test is a longitudinal compression. The subsequent image (Figure 4.2) displays the development of Young's modulus, where the displacement is $\Delta = 0.15\text{mm}$ which represents a deformation of 1% in the global model.

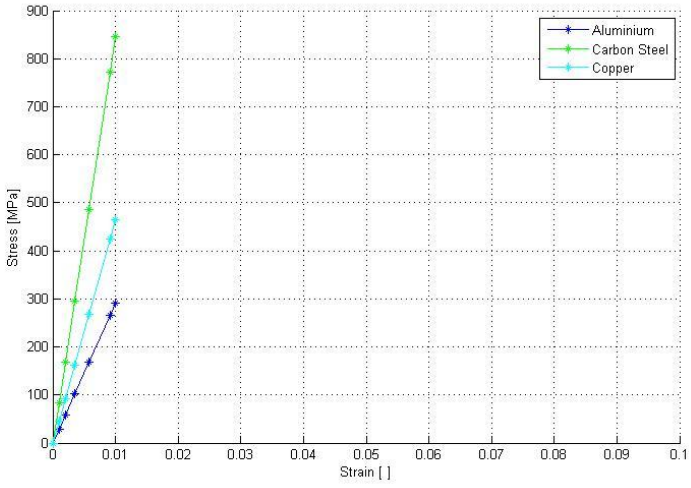

Figure 4.2 - Stress-Strain diagrams for whole specimen in each assigned material, elastic region, 1% deformation, longitudinal compression.

Table 4.2 presents the values of Young's modulus (calculated under the equation 4.5) that are associated with both the solid walls of the specimen and the specimen as a whole. The variation among this two assessments is the value used to calculate the area, as presented in proper table. When assessing the value for the specimen walls it was used the projected area related to the solid part, presented in Table 4.1 under the name "walls projected area". In order to evaluate the complete model Young's modulus it was used the projected area

including the cavities, as in Figure 4.1. This value is, as well, presented in Table 4.1 under the name “projected area”.

Table 4.2 - Obtained Young’s Modulus for each material, 1% deformation

Material	Solid part Young’s modulus [GPa]	Specimen Young’s modulus [GPa]
Aluminium	74.886	29.224
Carbon steel	217.38	84.510
Copper	119.56	46.481

For the solid part, the values are inside the range which is indicated for the base material. As stated in Figure 2.4, for a small deformation as 1%, the specimen is inside the quasi-linear elastic response area. Hence, the values achieved for the specimen Young’s modulus are expected to be minor than the base material ones.

From the observed variations in rotational displacement occurred in some cellular walls (Figure 4.3 to Figure 4.5), is conceivable to sustain that, for different materials, the specimen deformation will occur differently. Nevertheless, all the walls will experience deformation. Comparing the representations on the figures below, carbon steel was subjected to rotational displacements larger than the other two specimen materials. On the other hand, for all the assigned materials, these walls remained with the same structural organization, which is acceptable for 1% of deformation. Nevertheless, in the areas with greater values of rotational displacements, is likely that the cell walls will present more evident deformation mechanisms.

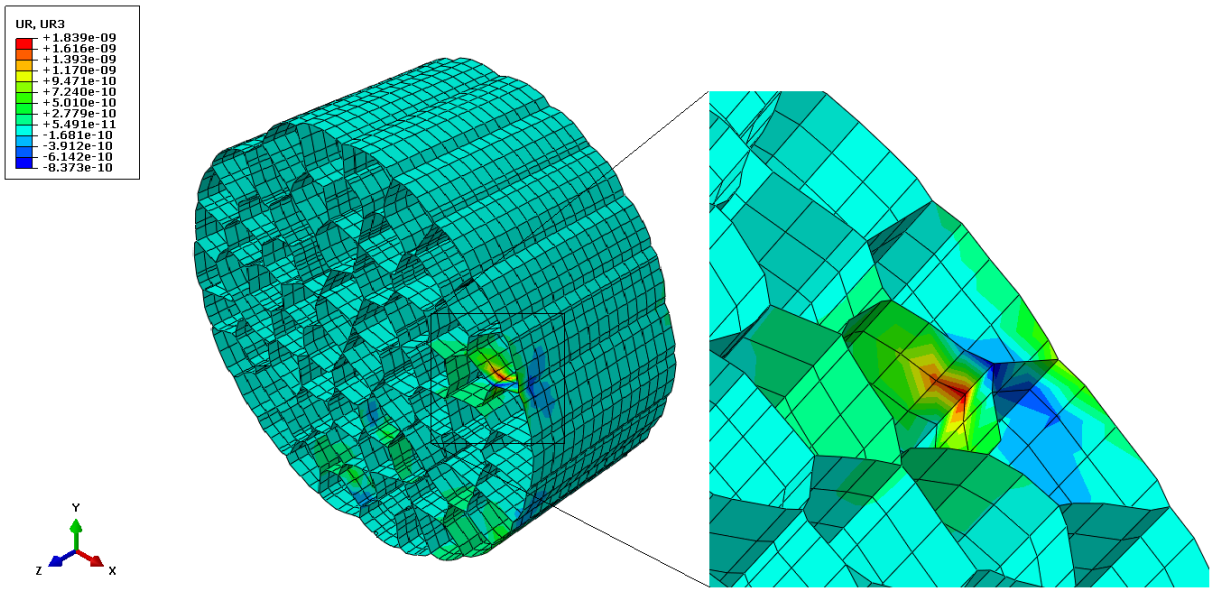

Figure 4.3 - Displacement magnitude variation [N] for prescribed displacement 0.15 mm, copper, ε=1%.

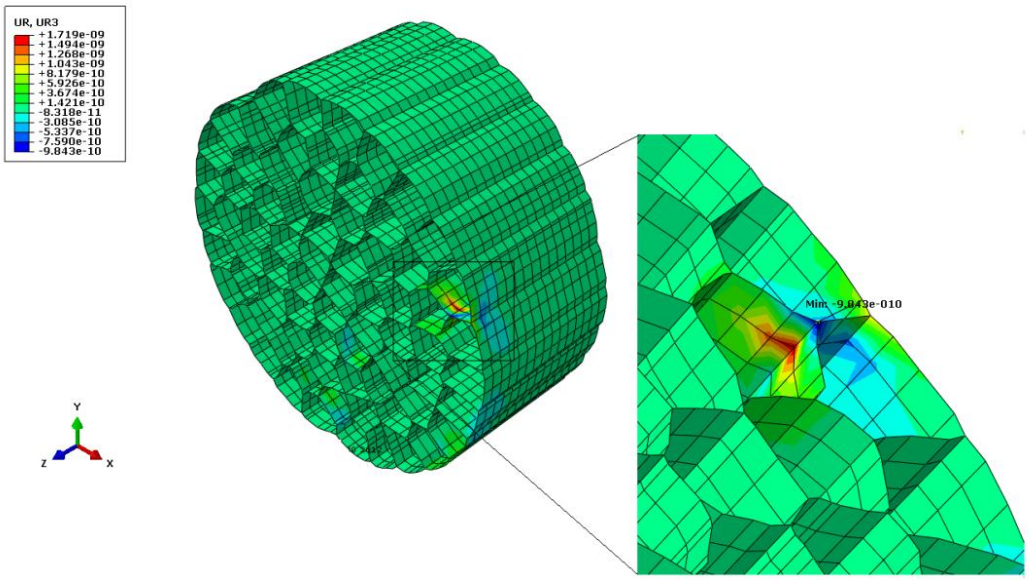

Figure 4.4 - Displacement magnitude variation [N] for carbon steel, $\boldsymbol{\varepsilon = 1\%}$, prescribed displacement 0.15 mm.

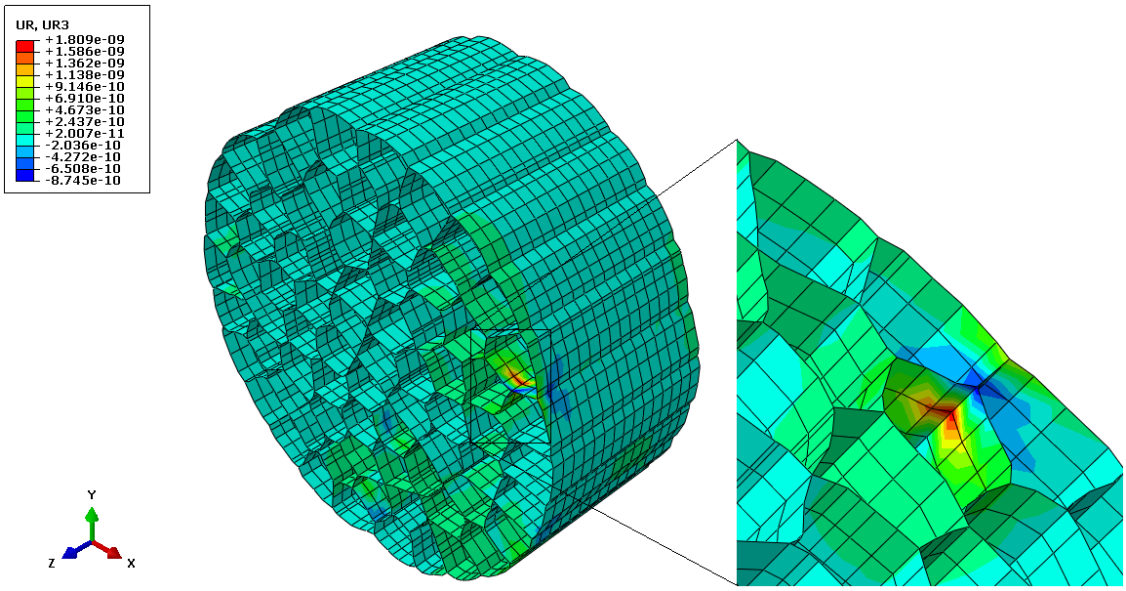

Figure 4.5 - Displacement magnitude variation [N] for aluminium, $\boldsymbol{\varepsilon = 1\%}$, prescribed displacement 0.15 mm.

The graphic in Figure 4.7 shows the reaction force in the direction of the load prescribed. The specimen was assigned with the elastic properties of copper material. The regions where larger reaction force values appear are positioned at the bottom, plane ZX.

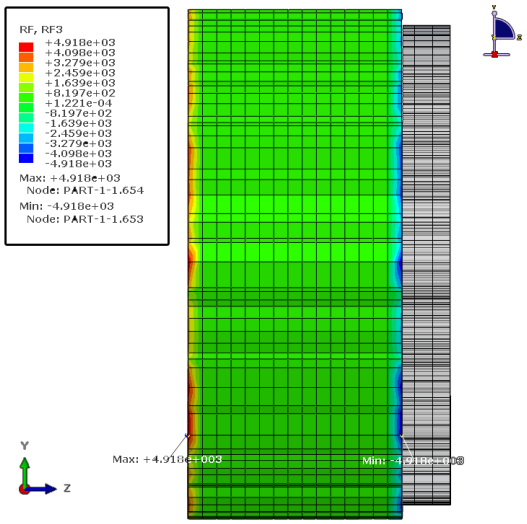

Figure 4.6 - Reaction force [N] in Z-direction, for elongation 1%, primary specimen in grey, assigned material copper.

4.4.2 Transverse Compression

The first displacement prescribed was $\Delta l = 0.3$ mm, which corresponded to $\varepsilon = 1\%$ of deformation. The load was divided into 38 increments determined automatically by the ABAQUS® software method. For the output data of the transverse compression numerical analysis, the node selected corresponded to the reference point in the bottom plate. The reactions in Figure 4.6 are taken from the reference point (RF) in the bottom plate as well.

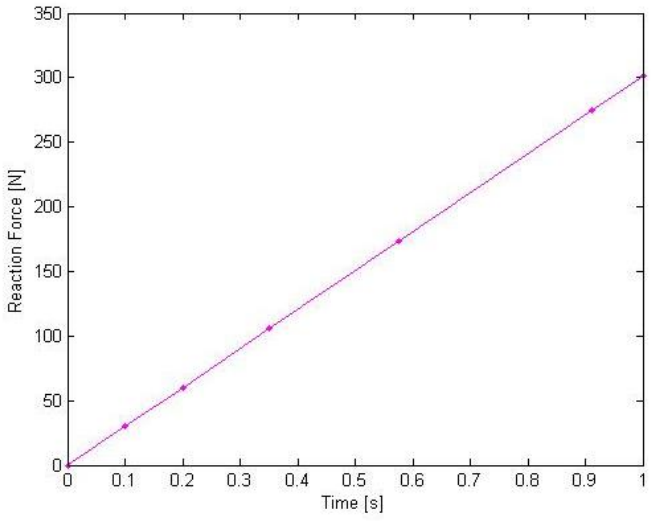

Figure 4.7 - Total reaction force distribution, assigned material, copper, ε=1%.

For this numerical essay, the specimen was subjected to different levels of displacement. The purpose was to assess at which value would begin the transition zone, where the cellular materials first exhibit buckling, plastic deformation and collapse of intercellular walls. This value was obtained for $\Delta = 2.5$mm which corresponded to a deformation of the global model $\varepsilon = 8.3\%$. The true stress-strain curves achieved are represented in Figure 4.9.

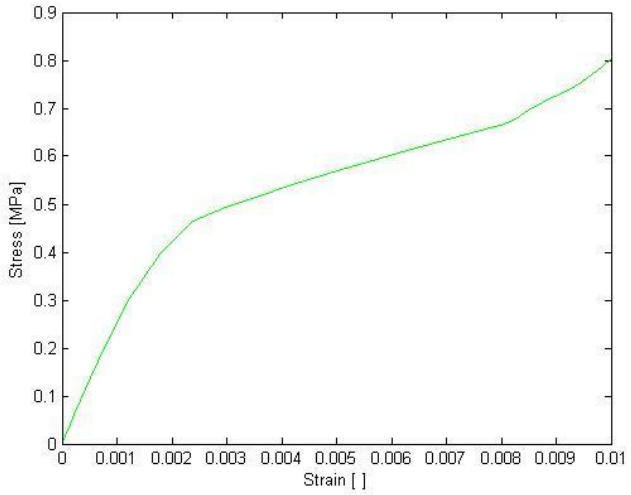

Figure 4.8 - Engineering stress strain curve in detail for copper, ε =1%, obtained elasticity module with value E=86.9686 MPa.

To determine Young's modulus was used in the numerical model only elastic material properties, the values were based in Hooke's relation (equation 4.5) and which are related, naturally with engineering stress-strain values.

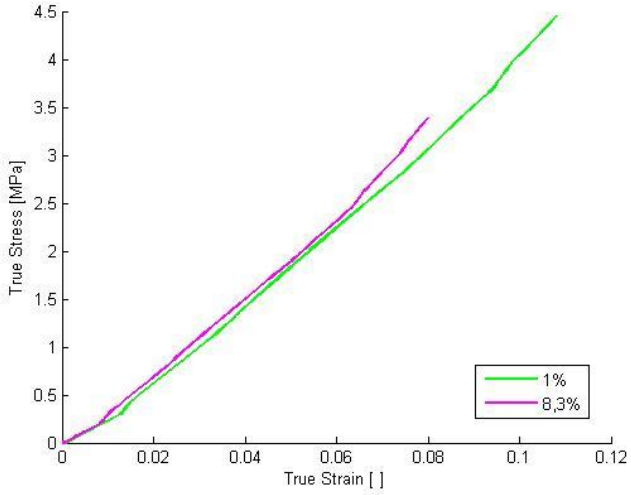

Figure 4.9 - True stress-strain curves for ε=1% and ε=8.3%

Once reached the transition zone limit, the plastic area started for the value which registered an increasing deformation in stress variation. After this, the internal structure of the model reorganized itself and the material presented a new variation of stress with specific strain, however in a non-linear way.

4.2 Plastic analysis

Substantial changes in geometry during the deformation process of the model are expected in this study. Stress values are not directly proportional to strain values and this corresponds to

non-linearity. This way, linear analysis appeared to be no longer the option to achieve accurate results.

Table 4.3- Phosphorous deoxidized copper plastic properties additionally prescribed.

Plastic properties	
Yield Stress[MPa]	Plastic Strain
180	0
216	0.1823
546	1.823

4.2.2 Transverse Compression

Nominal strain values are derived from the original specimen length. At small strains, errors in strain values arise through non-uniformity of the strain along the specimen by this loading method. However, the performance of the specimen under plastic deformation has most interest from this test. At small strains, error margin in plastic strains will be larger. However should become smaller at larger plastic strains.

The distribution of Von Mises stress in the model is represented in Figure 4.11. Greater values are localized in the contact area with the moving plate and in the central area of the model. In this case, the displacement prescribed was the one that conducted to the computational termination, $\Delta = 2.5\,\text{mm}$, which represents a displacement of 8,3%. The distribution of Von Mises stresses points to high values for the faces that suffered greater deformation rate.

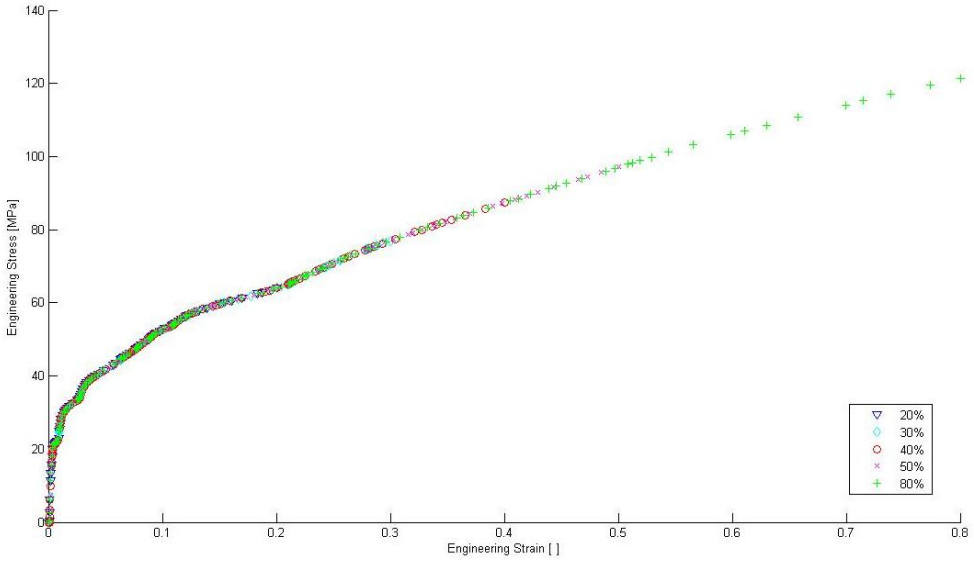

Figure 4.10 - Engineering stress-strain curves for transverse compression until 80% of displacement.

Moreover, the points where the walls coincide present, in most cases, higher concentration of stress. Nonetheless, for deformations until $\varepsilon = 8.3\%$, this referred points do not change outstandingly its geometry. After $\varepsilon = 8.3\%$, can be verified that the model undergoes in

plastic deformation mostly where the walls coincide, higher values of displacement result in rising values in the same walls. In Figure 4.12 is possible to verify the plastic areas of the specimen when the model undergoes a displacement of $\varepsilon = 40\%$.

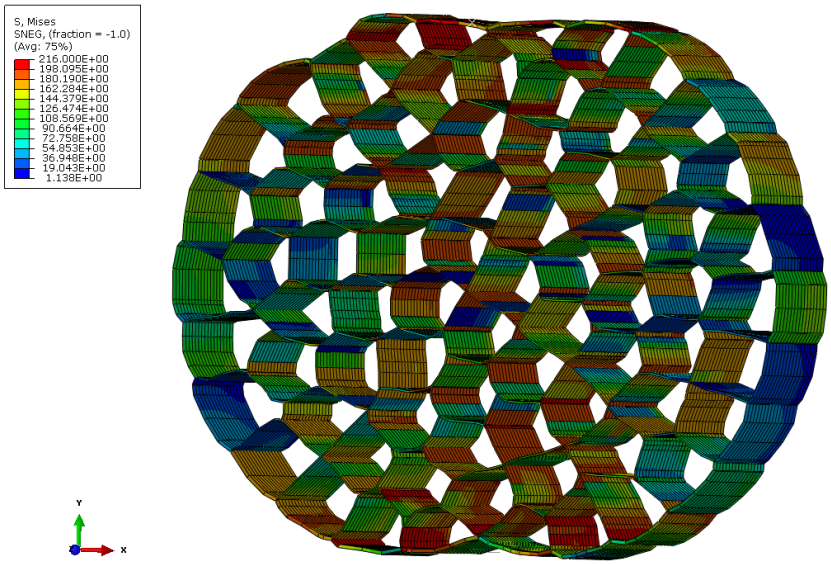

Figure 4.11 - Model deformation with Von Mises stress distribution, values in [N], (render wall thickness 0.04),

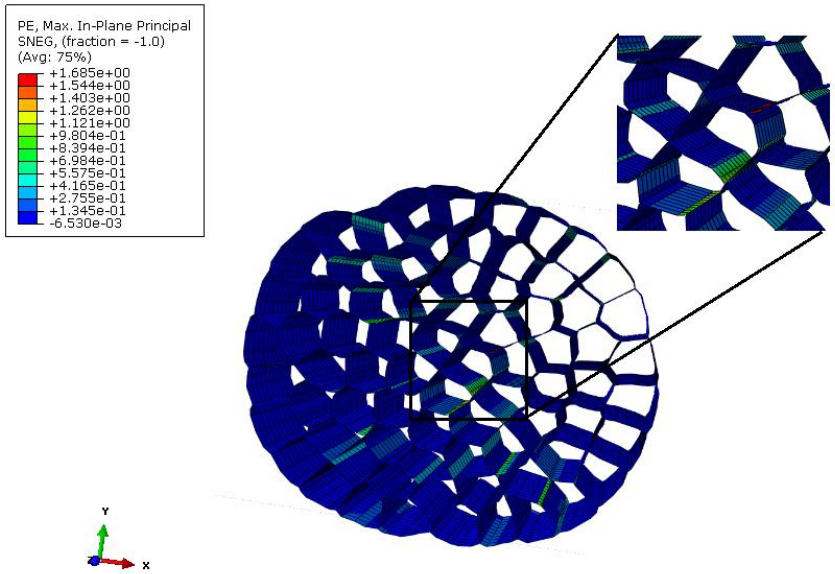

Figure 4.12 - Plastic deformation for a displacement of 40%, detail for the areas with higher plastic deformation (in red).

4.3 Thickness variation

As part of the investigation, thickness variation, which is related to the porosity of the material, will provide further information about the cellular specimen behaviour.

In this numerical procedure the material set in ABAQUS was phosphorous deoxidized copper. This slight change in the parameters was motivated by the fact that both the original model and later, the experimental specimens were produced in the referred material. The properties added in the material description are exposed in Table 4.4 and Table 4.5.

Table 4.4 - Phosphorous deoxidized copper elastic properties described in the numerical model.

Elastic properties	
Young's modulus	Poisson's ratio
110 000	0.343

Table 4.5 - Phosphorous deoxidized copper plastic properties described in the numerical model.

Plastic properties	
Yield Stress[MPa]	Plastic Strain
180	0
216	0.1823

Regarding the thickness variation and subsequent alteration in the specimen porosity, the obtained results were gathered in **Erro! A origem da referência não foi encontrada.** The assessment of the specimen volume was performed through ABAQUS® information tool. Once the thickness variation influences on the weight and volume of the specimen and the available information regards just the volume, some modifications took place for the calculus of porosity. Hence, using equation 2.1 and bearing in mind that $\rho = {}^{m}/_{V}$:

$$\rho_R = \frac{\rho^*}{\rho_s} = \frac{{}^{m^*}/_{V^*}}{{}^{m_S}/_{V_S}} \tag{4.1}$$

Once the voids are filled with air, and assuming that this value does not make influence on the weight, $m^* = m_S$

$$\rho_R = \frac{V_S}{V^*} \tag{4.2}$$

In this step is important to denote the assumption concerning the volume of the specimen, V^*. Despite the thickness variation of the outer wall of the specimen, it was assumed that the model was always produced with an outer tube with the same diameter (30mm), as a result, the volume of the specimen would remain equal. The value for $V^* = 10163.90525$ was obtained through CATIA®.

In Table 4.6 is possible to verify that less porous materials are correspondent with the thicker

inner wall (0.6mm). Further relations will be established after collecting the stress strain curves for each variation.

Table 4.6 - Thickness variation and assessment of porosity (Phosphorous deoxidized copper).

Walls thickness[mm]	Solid part volume V_S [mm^3]	ρ_R	Porosity
T4 - t2	4029	0.3964028	0.60359725
T1 – t 0.2	2425.10	0.2385992	0.76140077
T1 – t 0.4	3520.47	0.3463698	0.65363018
T1. – t 0.6	4615.84	0.4541404	0.5458596
T1.5 – t 0.2	3089.97	0.3040141	0.69598595
T1.5 – t 0.4	4185.34	0.4117846	0.58821537
T1.5 – t 0.6	5280.71	0.5195552	0.48044478
T2 – t 0.2	3754.84	0.3694289	0.63057113
T2 – t 0.4	4850.21	0.4771995	0.52280055
T2 – t 0.6	5945.58	0.58497	0.41502997

Regarding the stress-strain curves for each thickness variation of the specimen, assigned with the properties in Table 4.4 and Table 4.5. The curves obtained are identified by colours depending on the inner wall and by their contour according to the outer wall thickness; this layout is visually explained in the legend of each representation.

Observing the characteristics of the stress-strain diagrams for the thickness wall variation it is possible to infer that the thickness of the outer wall is not, for itself, a preponderant feature that can influence mechanical behaviour. When the inner wall presents a thickness $t = 0.6$ mm (marked in blue), the model has greater Young's Modulus, clearly, if the outer wall is thicker, then the Young's modulus will be, as well higher.

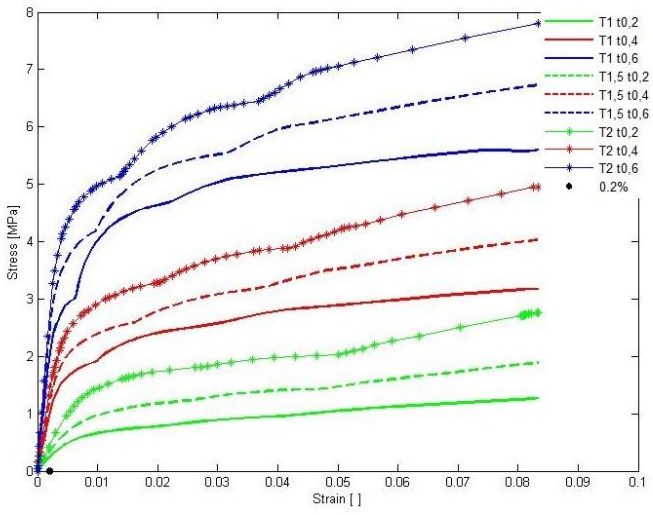

Figure 4.13 - Stress strain curves for each variation of wall thickness for UniPore structure (Phosphorous deoxidized copper).

The combination between inner and outer wall thickness, changes that will provide different porosities, give UniPore material a specific resistance. UniPore material will be more or less stiff to an applied force according to both inner and outer wall thickness, which is, as well, related with the porosity.

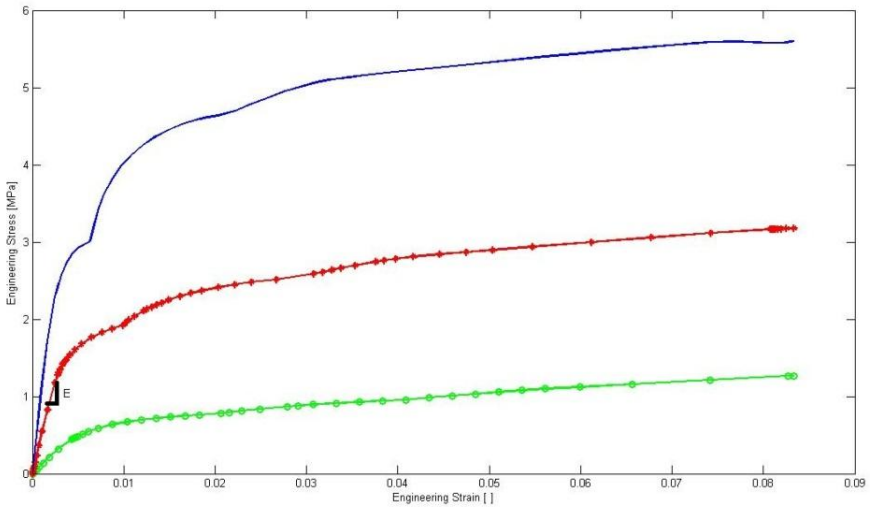

Figure 4.14 - Representation for obtained value of Engineering Modulus of Elasticity, marked with E in the red line, stress-strain curves for 1mm of outer wall thickness, and for 0.2, 0.4 and 0.6 inner wall thickness.

The subsequent Table 4.7 presents the values for Young's modulus as well as the yield stress, point where the structure started to deform plastically. Once this point is surpassed, some fraction of deformation becomes permanent and irreversible. The stiffness of the model is higher at less porous structures.

Table 4.7 - Compilation of Young's modulus values according to each thickness (Phosphorous deoxidized copper).

Thickness of (*T*) outer – (*t*) inner wall[mm]	Young's Modulus [MPa]	Yield Strength [MPa]
T1 – t 0.2	21.0444	0.58
T1 – t 0.4	47.6316	1.6
T1. – t 0.6	91.1293	2.85
T1.5 – t 0.2	31.7290	0.98
T1.5 – t 0.4	72.6171	2.22
T1.5 – t 0.6	137.4582	3.90
T2 – t 0.2	39.0397	1.35
T2 – t 0.4	86.0594	2.5
T2 – t 0.6	162.5054	4.5

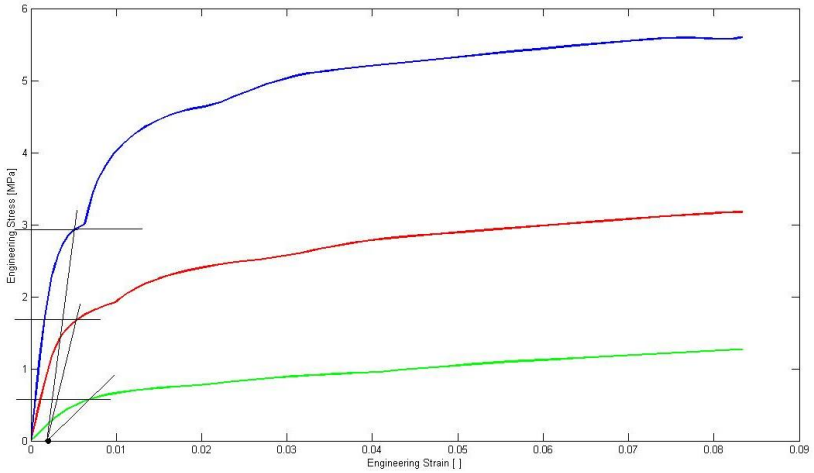

Figure 4.15 - Yield strength, using 0.2% offset method, exemplification for three stress strain curves, black dot marks value 0.002.

A structure with porosity 0.41, the less porous, presented the greater value of yield strength, which means that the necessary stress to be applied in order to start a permanent deformation would be as small as the porosity of the model. For very porous material samples, the yield strength would be as small as porosity.

After undergoing the transition zone, the UniPore samples start to present increasingly visible deformations in its cellular structure. From Figure 4.3 to Figure 4.5 is possible to visually compare the dissimilarities in each model depending on the wall thickness of the structure. All structures are represented in a cross sectional view of the model in order to identify and compare distortions easily. As expected, for this level of displacement, in the transition zone, the deformation mechanisms endured by the walls in the model can be identified as stretching or sliding distortions, Figure 4.18. Although, for greater displacements, is expectable to observe also distortion by sliding and more evident mechanisms of collapse.

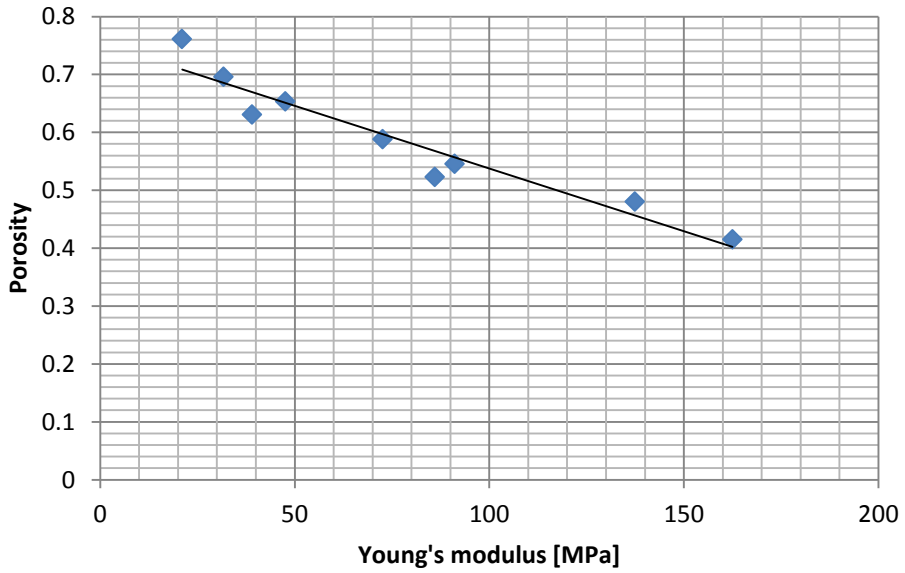

Figure 4.16 - Young's modulus variation within porosity.

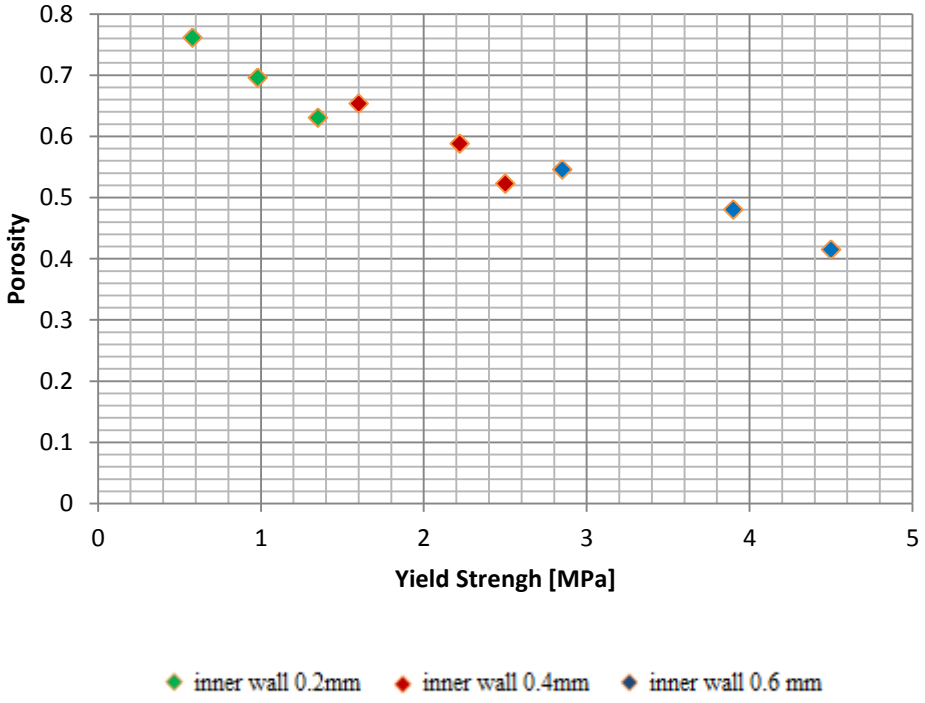

Figure 4.17 - Yield strength variation with specimen porosity.

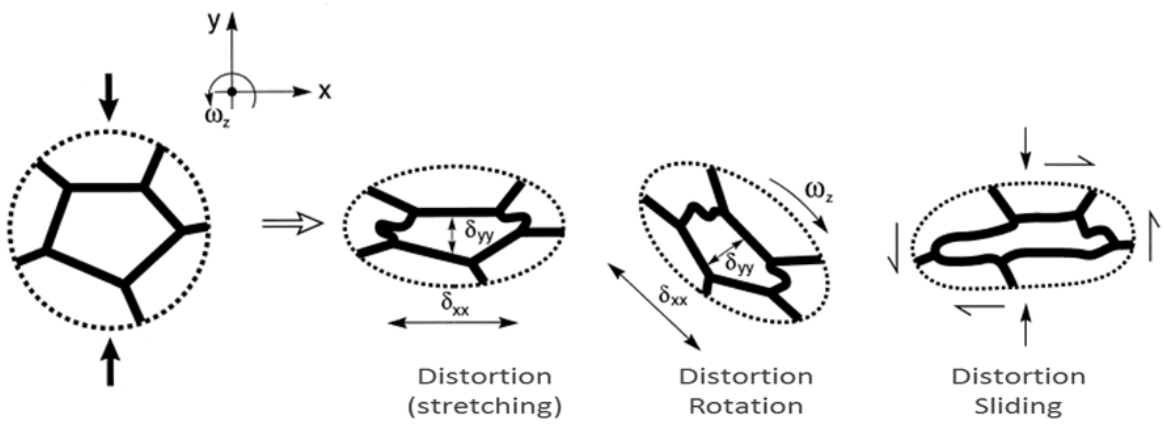

Figure 4.18 – Schematization of deformation mechanisms in cellular walls.

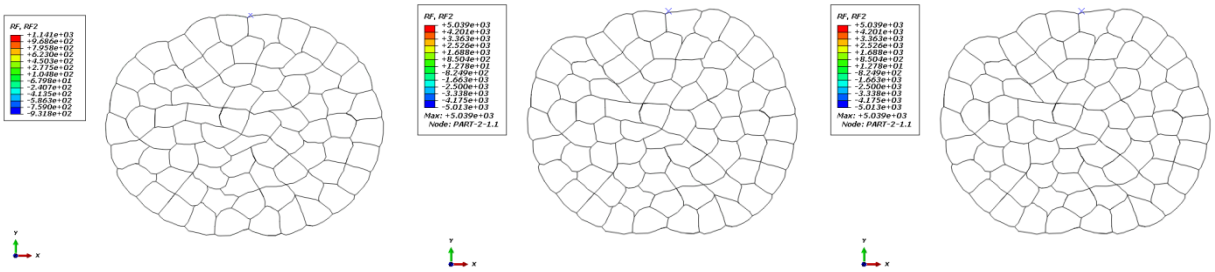

Inner wall 0.2mm Inner wall 0.4mm Inner wall 0.6mm

Figure 4.19 - Variation in structure for outer wall thickness 1mm and 8.3% displacement.

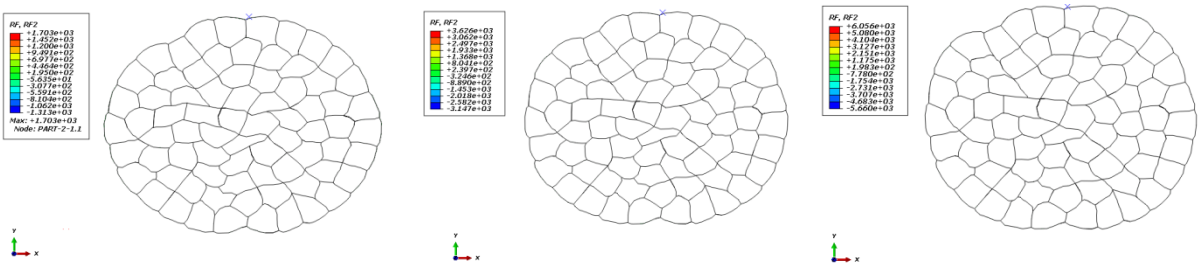

Inner wall 0.2mm Inner wall 0.4mm Inner wall 0.6mm

Figure 4.20 - Variation in structure for outer wall thickness 1,5mm and 8.3% displacement.

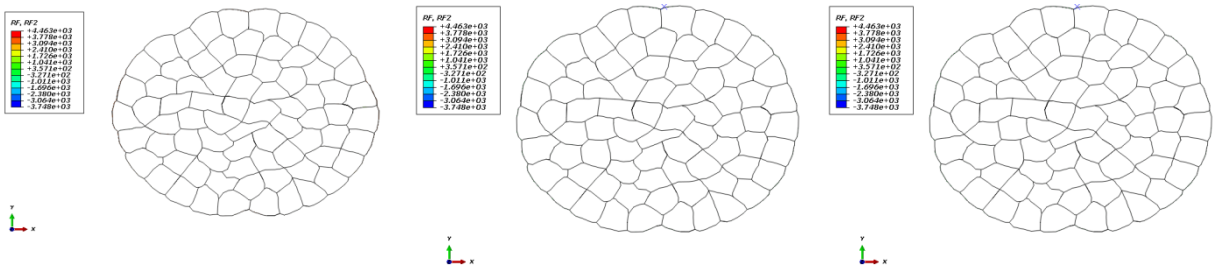

Inner wall 0.2mm Inner wall 0.4mm Inner wall 0.6mm

Figure 4.21 - Variation in structure for outer wall thickness 2mm and 8.3% displacement.

4.2.3 Elastoplastic behaviour compared with experimental results

In order to verify the result was established a comparison between real specimen and a corresponding numerical essay. The results show some differences, while some may be justified by the fact that UniPore model is a stochastic material, even though with some control of the geometry.

As showed in Figure 4.22 the specimen starts to exhibit some plastic deformation and disaggregation of intracellular walls, situation that gets even more evident in the subsequent essay, Figure 4.23.

Finally it is presented a picture of the model in the advanced stage of stress plateau, where the cellular walls are touching and the stiffness of the material increases gradually.

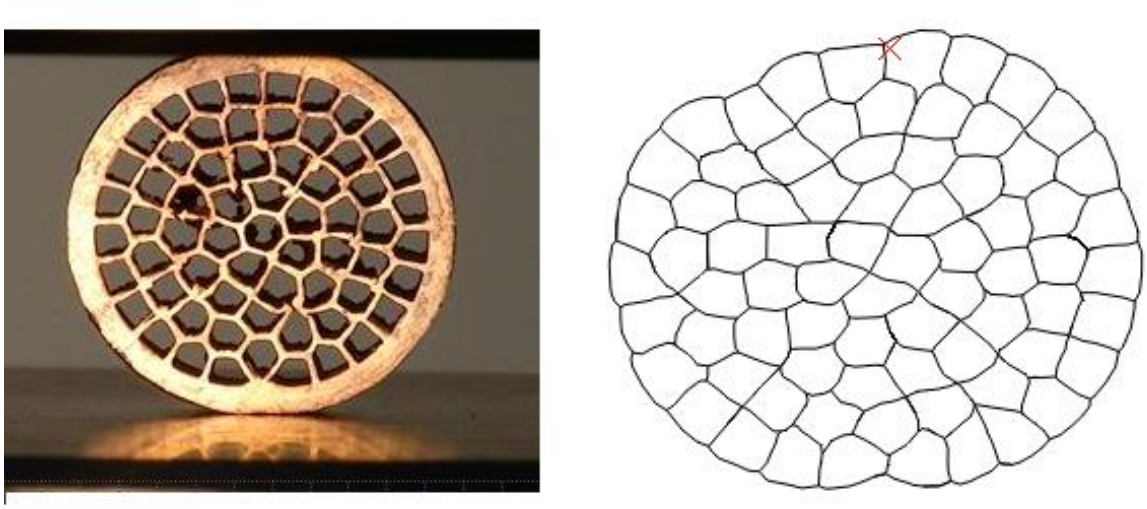

Figure 4.22 - UniPore sample under compression, right after transition zone (left) and numerical model (right), in intermediate step.

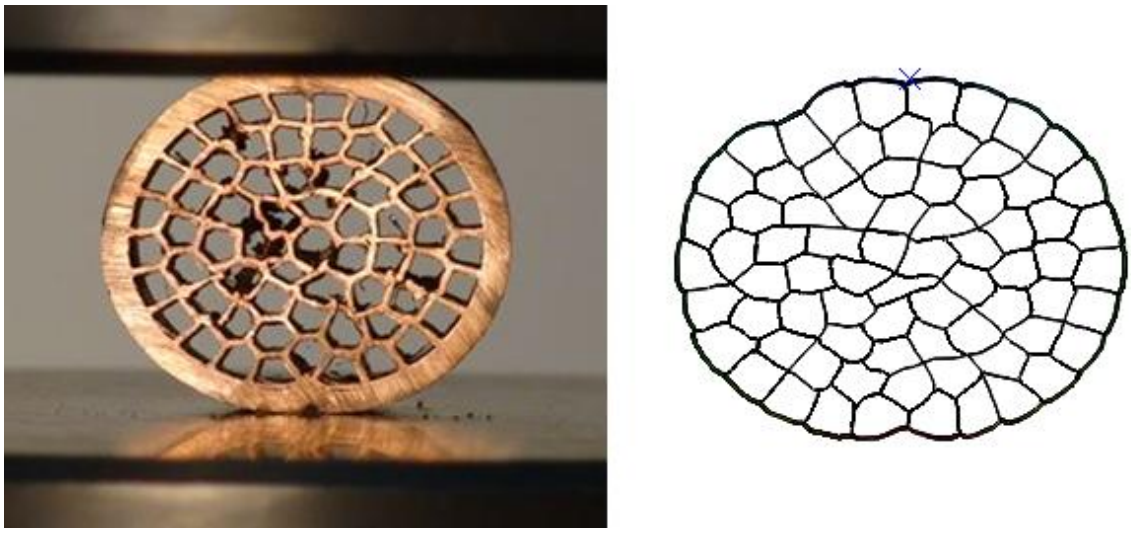

Figure 4.23 - Marked collapse of intracellular walls in experimental model (left) and experimental model (right), for 8,3% of displacement (transition zone)

Figure 4.24 - Collapsed UniPore sample

5. DISCUSSION

The significance of this work goes in the direction of substantiate the experimental data to be determined on the engineering module of elasticity of the prescribed materials. This stage has made forward to a better understanding of the mechanical behaviour of UniPore cellular material.

An orthotropic material has two or three mutually orthogonal double axes of rotational symmetry so that its mechanical properties are, generally, different along each axis. Orthotropic materials are thus anisotropic; their properties depend on the direction in which they are measured. An isotropic material, in contrast, has the same properties in every direction. UniPore material is and anisotropic and orthotropic material. The strength and stiffness of this material are generally greater in a direction parallel to the pores than in the transverse direction.

Transverse compression testing is a useful procedure for measuring the plastic flow behaviour and ductile fracture limits in materials. Measuring the plastic flow behaviour requires frictionless (homogeneous compression) test conditions, which are not difficult to achieve with the computer simulation but will cause dissimilarities in the physical essays. This compression test is also useful for measurement of elastic and compressive fracture properties of materials as UniPore cellular material.

A significant assumption to be attained is the limitation inherent to the linear analysis performed, once this regimen occurs only for a short period of the stress-strain curve. Bearing in mind this limitation, seemed appropriate to clarify the mechanical behaviour of UniPore material performing a non-linear analysis, once this regimen takes place in a large part of the curve. Another point that should be mentioned is related with the low values for Young's Modulus, this is related with the cellular structure in the longitudinal direction

Under longitudinal loading the yield surfaces progresses in an approximately geometrically self-similar way, while under transversal loading the yield surfaces elongate. This deformation patterns are very complex and vary not only with this elongation, minor changes in the final model are produced in all directions.

For the transversal compression test, the friction forces on the top and bottom of the specimen might cause an imbalance of forces in the horizontal direction, Z direction. This is implied by internal horizontal forces acting on the vertical faces of the specimen to maintain force equilibrium so that the specimen did not slide; these forces are related with the boundary conditions prescribed.

In addition, to verify that both strength and stiffness of this material are greater in a parallel direction to the pores than in the transverse direction it is acceptable that this last gives the model a larger ability to deform.

The numerical results point that, in longitudinal compression, the specific geometry design of UniPore material does not affect the stiffness of the material, which is considered

remaining identical along the displacement variation. In compression, all models show a linear-elastic regime followed by a plateau of roughly constant stress, leading into a last regime of suddenly rising stress.

As predictable, the value of Young's modulus registers a growth with increasing value of wall thickness, which is directly related with the material porosity. The thicker the wall the less porous is the specimen. This means that depending on the application purpose for the UniPore cellular material would be appropriate to use smaller wall thicknesses for a desired structural very deformable application that could absorb energy, or thick walls for applications that desire a less deformable structure. UniPore could also have functional applications, taking advantage of the base material properties or even a possible combination where this novel material can both satisfy some functional and structural requirements.

Young's modulus describes how well the specimen maintains its length when compressed. It is also a measure of stiffness. Therefore as aluminium has the smaller value of Young's modulus, means that is more easily stretched then copper or carbon steel, since less stress is needed to achieve a given strain. For instance, a UniPore model with aluminium material and minor wall thicknesses would be very deformable in transverse compression and either very deformable under a longitudinal compression.

Upon an experimental essay, differences in some numerical values can be perhaps due to deviations of the description of topology and pore morphology of the real situation. Generally, engineering modulus in longitudinal direction is greater than in the transverse direction, which is expected, since the material is structurally more weakened in the transverse than in longitudinal direction, due to his geometry. In transverse load model, a compressive stress is applied from the outside to the remaining locations on the model walls due to outside pressure, which is related with the cells elongation and weakens the structure.

6. CONCLUSIONS

Cellular materials have remarkable properties and the number of possible applications will develop along with the full knowledge in manufacture and characterize these materials in an accurate and precise way. Blast welding can be an option to produce cellular materials with more deterministic geometry. However there are many experimental procedures to endure as well as other numerical investigations. This investigation work intended to be of some help in the knowledge of this new cellular material properties.

The numerical analysis proved to be a good alternative to experimental testing. Despite the fact that the real geometrical characteristics of UniPore cellular material could not be more precisely defined, this thesis work established a good approximation to determine the mechanical properties of UniPore cellular material. Within this thesis investigation mechanical properties and behaviour characteristics of UniPore material were collected. This work also presents a good basis for further numerical studies of materials with identical characteristics as well as valid data for the experimental essays yet to be performed. The purpose and objectives of the thesis were therefore satisfied.

7. LITERATURE

[1] M. F. Ashby, A. G. Evans, N. A. Fleck, L. J. Gibson, J. W. Hutchinson and H. N. G. Wadley, Metal Foams: A Design Guide, Butterworth Heinemann, 2000.

[2] I. Duarte and M. Correia, "Aluminium Alloy Foams: Production and Properties, Powder Metallurgy," 2012.

[3] B. Sosnick, "Process for making foamlike mass of metal". United States of America Patent 2,434,775, 20th Jan. 1948.

[4] J. Baumeister and H. Schrader, "Methods for manufacturing foamable metal bodies". Bremen Patent 5,151,246, 31 May 1991.

[5] J. Banhart and J. Baumeister, Production methods for metallic foams, Warrendale, 1988.

[6] E. J. R. Johan Bjorksten, "CONTINUOUS PROCESS FOR PREPARING UNIDIRECTIONALLY REINFORCED METAL FOAM". United States of America Patent 3941182, 2 Mar 1976.

[7] L. J. Gibson and M. F. Ashby, Cellular Solids structure and properties, 2nd ed., Cambridge, 1997.

[8] H.-P. Degischer and B. Kriszt, Eds., Handbook of Cellular Metals: Production, Processing, Applications., Wein: Wiley-VCH, 2002.

[9] J. Banhart, "Manufacture, characterisation and application of cellular metals and metal foams," in *Progress in Materials Science*, Fraunhofer, Germany, Elsevier, 2001, p. Pages 559–632.

[10] C. . B. Williams, "Design and Development of a Layer-Based Additive," Georgia, 2008.

[11] H.-P. Degischer and B. Kriszt, Eds., Handbook of Cellular Metals: Production, Processing, Appications., Wein: Wiley-VCH, 2002.

[12] B. Fosi, "brunofosi.com," february 2008. [Online]. Available: http://brunofosi.com/wp-content/files/voronoi-chair-1-diagram-680x378.jpg. [Accessed 2012].

[13] D. Austin, "American Mathematical Society," Percolation: Slipping through the Cracks, 2012. [Online]. Available: http://www.ams.org/samplings/feature-

column/fcarc-percolation. [Accessed 2012].

[14] C. B. W. A. D. Nicholas A. Meisel, "LIGHTWEIGHT METAL CELLULAR STRUCTURES VIA INDIRECT 3D PRINTING," pp. 162-176, August 2012.

[15] M. J. A. S. J. B. T. Studnitzky, "3D-printing as manufacturing method for cellular materials," in *CELLMAT*, Dresden, Germany, 2012.

[16] O. W. Blodgett and D. K. Miller, "Manufacturing Processes," p. 76.

[17] K. H. Z. R. Matej Vesenjak, "Computational Simulations of Unidirectional Cellular Material UniPore subjected to Dynamic Loading," in *DYNAmore*, Stuttgart, 2013.

[18] V. M., K.-O. L., R. Z. and Ö. A., "Experimental Study of Open-Cell Cellular Structures," *Experimental Mechanics*, pp. 501-509, 08 October 2009.

[19] I. Duarte, "Espumas metálicas: Processo de fabrico, caracterização e simulação numérica," Porto, 2005.

[20] B. P. Lopes, "Development of percursors to produce metallic foams," Aveiro, 2001.

[21] J. S. Rao, "Finite Element Methods," in *History of Mechanism and Machine Science*, vol. 20, Springer Netherlands, 2011, pp. 141-183.

[22] C. C. J. K. A. D. M. a. F. M. M. Seepersad, "Robust Design of Cellular Materials with Topological and Dimensional Imperfections," *Journal of Mechanical Design*, vol. 128, pp. 1285-1297, 2006.

[23] S. C. H. M. H. C. D. M. J. K. A. a. F. M. M. Thompson, "Robust Materials Design of Blast Resistant Panels," in *IAA/ISSMO Multidisciplinary Analysis and Optimization Conference*, Portsmouth, 2006.

[24] A. A. A. Mousavi, W. B. Brown, S. J. Burley and S. T. S. Al-Hassani, "Simulation of Explosive Welding with ANFO Mixtures," *SMEIR*.

[25] V. G. Fernández, "TDX - Thesis doctorals en Xarxa," 2001. [Online]. Available: http://www.tdx.cat/bitstream/handle/10803/6043/03Vggf03de11.pdf;jsessionid=428A3494C49E634E19657390C7BC3B1E.tdx2?sequence=3. [Accessed November 2012].

[26] L. L. Hill, S. J. Crosier, T. R. Smith and M. Goodchild, "A Content Standard for Computational Models," *D-Lib Magazine*, vol. Volume 7, June 2001.

[27] MatWeb, "Online Materials Information Resource - MatWeb," MatWeb, 1996. [Online]. Available: http://www.matweb.com/. [Accessed 9 March 2012].

[28] M. Bedford and W. Fowler, Engineering Mechanics, Addison-Wesley Longman, 1999, pp. 503-553.

[29] (. S. C. Roylance David, "MIT Open Courseware," MIT, 2002. [Online]. Available: http://ocw.mit.edu/courses/materials-science-and-engineering/3-11-mechanics-of-materials-fall-1999/modules/#jv. [Accessed August 2012].

[30] M. Vesenjak, T. Fiedler, Z. Ren and A. Öchsner, "Behaviour of Syntactic and Partial Hollow Sphere Structures under Dynamic Loading," *ADVANCED ENGINEERING MATERIALS,* vol. 10, 2008.

[31] F. Ramsteiner, N. Fell and S. Forster, "Testing the deformation behaviour of polymer foams," *Polymer Testing,* vol. Volume 20, no. Material Behaviour, p. 661–670, 23 May 2001.

[32] AZoM, "About AZoM - A Materials Information Encyclopedia/Resource," 2000. [Online]. Available: http://www.azom.com/images/Article_Images/ImageForArticle_5940(2).jpg. [Accessed November 2012].